

## 1 The genetic and dietary landscape of the muscle insulin signalling network

2  
3 Julian van Gerwen<sup>1</sup>, Stewart W. C. Masson<sup>1</sup>, Harry B. Cutler<sup>1</sup>, Alexis Díaz-Vegas<sup>1</sup>, Meg Potter<sup>1</sup>, Jacqueline  
4 Stöckli<sup>1</sup>, Søren Madsen<sup>1</sup>, Marin E. Nelson<sup>1</sup>, Sean J. Humphrey<sup>1</sup>, David E. James<sup>1,2,3</sup>  
5

6 1. Charles Perkins Centre, School of Life and Environmental Sciences, University of Sydney, 2006, Australia

7 2. Faculty of Medicine and Health, University of Sydney, 2006, Australia

8 3. Lead contact

9 Correspondence:

10 [david.james@sydney.edu.au](mailto:david.james@sydney.edu.au)

11 [sean.humphrey@mcri.edu.au](mailto:sean.humphrey@mcri.edu.au)

### 12 **Abstract**

13 Metabolic disease is caused by a combination of genetic and environmental factors, yet few studies  
14 have examined how these factors influence signal transduction, a key mediator of metabolism. Using  
15 mass spectrometry-based phosphoproteomics, we quantified 23,126 phosphosites in skeletal muscle of  
16 five genetically distinct mouse strains in two dietary environments, with and without acute *in vivo*  
17 insulin stimulation. Almost half of the insulin-regulated phosphoproteome was modified by genetic  
18 background on an ordinary diet, and high-fat high-sugar feeding affected insulin signalling in a strain-  
19 dependent manner. Our data revealed coregulated subnetworks within the insulin signalling pathway,  
20 expanding our understanding of the pathway's organisation. Furthermore, associating diverse signalling  
21 responses with insulin-stimulated glucose uptake uncovered regulators of muscle insulin  
22 responsiveness, including the regulatory phosphosite S469 on Pfkfb2, a key activator of glycolysis.  
23 Finally, we confirmed the role of glycolysis in modulating insulin action in insulin resistance. Our  
24 results underscore the significance of genetics in shaping global signalling responses and their  
25 adaptability to environmental changes, emphasizing the utility of studying biological diversity with  
26 phosphoproteomics to discover key regulatory mechanisms of complex traits.

29 **Introduction**

30 Protein post-translational modifications such as phosphorylation enable cells to rapidly respond to  
31 environmental changes by modifying protein function at low metabolic cost<sup>1</sup>. As a result of this high  
32 metabolic efficiency, phosphorylation is involved in nearly all biological processes and is dysregulated  
33 in numerous complex diseases<sup>2</sup>. Advances in mass spectrometry-based phosphoproteomics – the  
34 unbiased identification and quantification of protein phosphorylation – have led to the discovery of  
35 more than 100,000 phosphosites, revealing that the phosphoproteome comprises vast, interconnected  
36 phosphorylation networks<sup>3–6</sup>, rather than the textbook view of isolated, linear kinase cascades.

37 The insulin signalling network is among the most studied phosphorylation networks. Post-  
38 prandial increases in blood glucose stimulate pancreatic insulin secretion, coordinating a metabolic  
39 switch in target tissues like skeletal muscle and adipose<sup>7</sup>. Insulin increases glucose uptake into these  
40 tissues by promoting translocation of the glucose transporter GLUT4 to the plasma membrane, and  
41 serves other functions like enhancing protein synthesis, downregulating lipid catabolism, and altering  
42 gene transcription<sup>7</sup>. To coordinate these functions, insulin triggers a phosphorylation cascade primarily  
43 involving activation of the Ser/Thr kinase Akt, regulation of downstream kinases including mTORC1  
44 and GSK3, and modulation of parallel signalling arms<sup>7–9</sup>. Seminal phosphoproteomics studies  
45 demonstrated that this cascade regulates over a thousand phosphosites, with many still uncharacterised  
46 in insulin action<sup>10–12</sup>. Insulin resistance – the failure of insulin to promote glucose uptake in its target  
47 tissues – is triggered by genetic and environmental factors such as family history of metabolic disease  
48 and high-calorie diets<sup>13</sup>. Although insulin resistance is a major precursor of metabolic disease including  
49 type 2 diabetes, its mechanistic basis remains unresolved<sup>13–15</sup>.

50 Interactions between genetics and environment significantly regulate biomolecular processes,  
51 including insulin resistance<sup>16–19</sup>. As signalling pathways connect the extracellular environment to  
52 intracellular proteins, they are likely a major conduit of gene-by-environment interactions. Yet, how  
53 global phosphorylation signalling networks are regulated across different genetic backgrounds is  
54 relatively unexplored. Recent phosphoproteomics studies in yeast<sup>20</sup> and mice<sup>21</sup> identified genetic  
55 variants affecting multiple phosphosites, but did not analyse the phosphoproteome's response to acute  
56 perturbation, which is crucial to its role as a signal transduction system. We have also shown marked  
57 variation in acute signalling responses to exercise or insulin across individuals<sup>22</sup>. However, this study  
58 did not systematically assess the relative contributions of genetics and the environment<sup>22</sup>.  
59 Understanding how these variables intersect with signal transduction is fundamental to our basic  
60 knowledge of signalling and the advancement of personalised medicine, which advocates individualised  
61 treatment regimens based on genetic risk factors and gene-by-environment interactions<sup>16,23</sup>.

62 Inbred mice allow precise control of genetics and environment unachievable in human studies,  
63 enabling examination of how these factors interact to influence biomolecular systems<sup>24</sup>. Here, we  
64 performed phosphoproteomics on insulin-stimulated or control skeletal muscle from five genetically  
65 distinct inbred mouse strains fed either an ordinary chow diet or a high-fat, high-sugar “western style”

66 diet. Strikingly, we found that genetic background influenced both the phosphoproteomic insulin  
67 response of chow-fed mice, as well as how these responses were modified by high-fat, high-sugar  
68 feeding. These signalling changes were reflected in altered activity profiles of multiple kinases and  
69 provided insight into the functional organisation of the insulin signalling network by revealing  
70 subnetworks of coregulated phosphosites. A major challenge in phosphoproteomics studies is  
71 pinpointing important regulatory events among the many responding to a stimulus. We reasoned that  
72 associating changes in protein phosphorylation across the gene-by-environment landscape with  
73 phenotypic change – in this case insulin-stimulated glucose uptake – would dissect mechanistic targets  
74 with greater fidelity. This approach generated known as well as candidate regulators of insulin-  
75 stimulated glucose uptake, leading us to demonstrate that glycolytic upregulation reverses insulin  
76 resistance. Our work represents the first global portrait of insulin signalling network plasticity in  
77 response to genetic and environmental variation, which will serve as an important resource in future  
78 studies of insulin action and resistance.

79

## 80 **Results**

### 81 ***Phosphoproteomics of insulin signalling in mouse skeletal muscle***

82 To study how protein phosphorylation networks are affected by genetics and environment, we examined  
83 insulin signalling in five genetically distinct inbred mouse strains including four lab strains with diverse  
84 metabolic phenotypes (C57Bl6J, NOD, BXH9, and BXD34<sup>18</sup>), and the wild-derived CAST strain (**Fig. 1a**). Mice underwent a six-week diet regimen of standard lab diet (CHOW) or a high-fat high-sucrose  
85 diet (HFD), which is commonly used to induce insulin resistance<sup>18,25</sup>. Consistent with their diverse  
86 genetics, these strains differed in morphometric parameters (body weight, adiposity, lean mas) and  
87 metabolic traits (fasting blood glucose, fasting blood insulin, glucose tolerance) both on the CHOW  
88 diet and in their response to HFD-feeding (**Fig. S1**).

89 We focused on skeletal muscle, as it is the site of greatest post-prandial glucose uptake and the  
90 most significant contributor to impaired glucose disposal in type 2 diabetes<sup>26</sup>. Specifically, we chose to  
91 examine the soleus muscle, because its largely oxidative fibre composition resembles human muscle  
92 tissue more than other murine muscles<sup>27</sup>. Mice were injected retro-orbitally with saline control or insulin  
93 for 10 minutes, and the soleus was collected for phosphoproteomic analysis (**Fig. 1a**). A tritiated 2-  
94 deoxyglucose (<sup>3</sup>H-2DG) tracer was co-injected to measure soleus glucose uptake.

95 Using the EasyPhos workflow and data-independent acquisition (DIA) mass spectrometry<sup>28,29</sup>,  
96 we quantified 28,809 phosphopeptides across 95 biological samples, corresponding to 23,126 unique  
97 high-confidence phosphosites (Class I; localization score > 0.75) on 3,507 proteins (**Fig. 1b, Table S1**).  
98 On average we quantified 15,395 phosphopeptides in each sample (**Fig. S2a**). Due to the range in soleus  
99 mass across strains (**Fig. S1d**) we altered the protein material used for EasyPhos (C57Bl6J and NOD:  
100 755 µg, BXH9 and BXD34: 511 µg, CAST: 364 µg), though phosphopeptide quantification was  
101 minimally affected, with only 12.4% fewer phosphopeptides quantified on average in CAST compared

103 to the C57l6J/NOD (average 13891.56 vs 15851.29 **Fig. S2a**). Furthermore, while different strains  
104 clustered noticeably by the amount of protein material used, samples from animals of the same strain  
105 and diet were still highly correlated and generally clustered together, implying the data are reproducible  
106 (**Fig. S2b-d**).

107 To explore the soleus insulin signalling network, we examined phosphopeptides altered by  
108 insulin stimulation in at least one of the ten strain-diet combinations. First, to allow comparison across  
109 conditions, phosphopeptides were retained if they were quantified well enough to assess the effect of  
110 insulin in more than eight strain-diet combinations ( $\geq 3$  insulin-stimulated values and  $\geq 3$  unstimulated  
111 values in each combination). We then tested the resulting 10,432 highly quantified phosphopeptides for  
112 significant differences between unstimulated and insulin-stimulated samples (three-way ANOVA  
113 insulin main-effect q-value  $< 0.05$ ) that were of sufficient magnitude in at least one strain-diet  
114 combination (insulin/unstimulated fold change  $> 1.5$ ). This resulted in 441 insulin-regulated  
115 phosphopeptides on 232 proteins, which is noticeably more than recent studies of 10-minute insulin  
116 signalling in patient-derived myoblasts (174 phosphopeptides<sup>30</sup> and 242 phosphopeptides<sup>31</sup>) or mouse  
117 adipose tissue (319 phosphopeptides<sup>32</sup>) (**Fig. 1b, c, Table S1**).

118 Our analysis recovered many well-studied insulin-regulated phosphosites, including Akt  
119 substrates such as T247 on Akt1s1 (PRAS40), S939 on Tsc2, and S9 on Gsk3 $\beta$  (**Fig. 1d-f**), as well as  
120 targets of downstream kinases including the Gsk3 $\beta$  substrate S641 on Gys1 (**Fig. 1g**). Enrichment of  
121 Gene Ontology (GO) biological processes recapitulated canonical insulin signalling axes including  
122 “insulin receptor signaling pathway”, “phosphatidylinositol 3-kinase signaling”, “protein kinase B  
123 signaling”, and “TORC1 signaling”, and multiple pathways related to glucose metabolism, fatty acid  
124 metabolism, autophagy, and protein translation, reflecting known targets of insulin action (**Fig. S3a**).  
125 Furthermore, insulin-regulated phosphosites were enriched for insulin regulation in our previous human  
126 skeletal muscle phosphoproteome (fold enrichment = 4.22,  $p = 9.50 \times 10^{-24}$ , one-sided Fisher’s exact test,  
127 **Fig. S3b**)<sup>22</sup>. Despite this, only half of all insulin-regulated phosphopeptides (228/441) were previously  
128 annotated as insulin-regulated in the PhosphositePlus database<sup>33</sup> (**Fig. S3c**), highlighting the potential  
129 of our data to discover novel aspects of insulin signalling while recapitulating known components. In  
130 addition to insulin, exercise also promotes GLUT4 translocation in skeletal muscle<sup>34</sup>. We identified a  
131 small subset of phosphosites regulated by insulin in this study that were also regulated by exercise in  
132 two separate human phosphoproteomics studies<sup>22,35</sup> (**Fig. S3d, Table S2**, phosphosites: Eef2 T57 and  
133 T59, Mff S129 and S131, Larp1 S498, Tbc1d4 S324, Svil S300, Gys1 S645), providing a starting point  
134 for exploring conserved signalling regulators of GLUT4 translocation. Overall, our phosphoproteomics  
135 data provide a comprehensive and high-quality atlas of insulin signalling in mouse skeletal muscle.  
136

### 137 ***Genetics and diet modulate insulin signalling***

138 The influence of genetic and environmental variation on global insulin signalling responses is largely  
139 unknown. We therefore developed a pipeline to address this question using our phosphoproteomics data

140 (Fig. 2a). First, we converted the intensity values of each insulin-regulated phosphopeptide to “insulin  
141 response” values, by normalising insulin-stimulated data to the unstimulated median of the  
142 corresponding Strain-Diet combination. Since protein expression should not change within a 10 min  
143 insulin stimulation<sup>32</sup>, this allowed us to parse out protein abundance differences across strains and diets  
144 and focus solely on acute signalling processes. We then assessed the impact of genetics in CHOW-fed  
145 mice by identifying phosphopeptides with differing insulin responses in one or more strains compared  
146 to C57Bl6J (“Strain effect”). Lastly, we explored the effects of HFD-feeding on signalling as two types  
147 of “Diet effects”, either as a “Uniform diet effect” – where HFD-feeding affects each strain similarly –  
148 or a “StrainxDiet effect” – where its impact depends on the mouse strain. Analyses of “Strain effects”  
149 and “Diet effects” were performed separately, so a phosphopeptide could have both a Strain effect and  
150 a StrainxDiet/Uniform Diet effect.

151 Almost half of the 441 insulin-regulated phosphopeptides displayed a Strain effect (Fig. 2b,  
152 Table S1). These included phosphopeptides where C57Bl6J had a stronger insulin response than other  
153 strains, such as S15 on the RNA methyltransferase Rnmt (Fig. 2c), and phosphopeptides where C57Bl6J  
154 had a weaker insulin response, such as S48 on the vesicle fusion regulator Vamp3 (Fig. 2d). Vamp3  
155 S48 is predicted to be highly functional (functional score = 0.750<sup>36</sup>), its phosphorylation correlates with  
156 glucose uptake in insulin-stimulated and/or exercised human skeletal muscle<sup>22</sup>, and Vamp3  
157 overexpression rescues GLUT4 translocation in insulin resistance<sup>37</sup>, suggesting that this site may  
158 represent a genetically variable control point of GLUT4 trafficking. In general, insulin responses were  
159 weaker in the four remaining strains compared to C57Bl6J, though the extent of this trend was strain-  
160 dependent (Fig. 2e). In all, the strain-affected phosphopeptides reveal a unique fingerprint of insulin  
161 signalling within each strain (Fig. 2f), highlighting the complex and widespread effects of genetic  
162 variation on signalling networks.

163 We next examined the impact of HFD-feeding in insulin signalling. StrainxDiet effects were  
164 more prevalent than Uniform diet effects (110 vs 10 phosphopeptides, Fig. 2g, Table S1), suggesting  
165 that the molecular impact of dietary perturbation was strongly modulated by genetic background.  
166 StrainxDiet effects impacted known regulatory phosphosites such as the inhibitory site S78 on Map2k4,  
167 whose insulin response was attenuated by HFD-feeding only in C57Bl6J and CAST (Fig. 2h). Map2k4  
168 activates p38 and JNK kinases which have been implicated as drivers of HFD-induced insulin  
169 resistance<sup>8</sup>, and based on the behaviour of S78, the orchestration of this detrimental signalling axis in  
170 HFD-feeding may depend on genetic background.

171 HFD-feeding exerted complex effects on signalling, with the balance between suppressed and  
172 enhanced insulin responses varying across strains (Fig. 2i). Furthermore, insulin-regulated  
173 phosphopeptides were largely altered by HFD-feeding in only a single strain, and when multiple strains  
174 were affected, they often changed in opposite directions (Fig. 2j-k). For instance, multiple insulin  
175 responses were strengthened in BXH9 but weakened in C57Bl6J or CAST (Fig. 2k), such as S500 on  
176 the translation regulator Larp4b (Fig. S3e). Principal component analysis supported the highly divergent

177 impact of dietary perturbation, as HFD-feeding displaced each strain in a distinct direction in principal  
178 component space (**Fig. 2l**). StrainxDiet and Strain effects were driven by a mixture of changes to  
179 insulin-stimulated phosphorylation, unstimulated phosphorylation, or both, highlighting the complexity  
180 of these signalling alterations (**Fig. S3f-g**). This analysis demonstrates the pervasive role of genetics in  
181 shaping signalling networks, as genetic background profoundly modulated the effect of HFD-feeding  
182 on insulin signalling.

183

184

185 ***Exploring genetic and dietary modulation of the insulin signalling network***

186 To understand the insulin signalling circuitry and functional pathways modulated by genetics and diet,  
187 we curated a network of 160 insulin-regulated phosphosites, comprising sites from a knowledge  
188 pathway-derived list of canonical insulin signalling proteins<sup>22</sup> and substrates of insulin-regulated  
189 kinases (**Fig. 3**, see Methods). Strain and diet affected multiple highly studied signalling sites, including  
190 Tsc2 S939 (Diet effect), Gsk3 $\alpha$  S21 (Strain and Diet effects), and Tbc1d4 T649 (Strain and Diet effects),  
191 while other sites such as Gsk3 $\beta$  S9 and Akt1s1 T247 were unaffected. Interestingly, strain and diet  
192 affected both canonical and non-canonical insulin signalling proteins to a similar extent (**Fig. S3h-i**).  
193 Non-canonical phosphosites could shed light on underappreciated outcomes of insulin action either  
194 altered or unaffected by genetics and the environment, such as the p70S6K substrate S47 on Dnajc2  
195 (Strain and Diet effects), which drives cellular senescence<sup>38</sup>, and S315 on Pcyt1a (no Strain or Diet  
196 effect), which inhibits phosphatidylcholine biosynthesis<sup>39</sup> (**Fig. 3**).

197 No functional pathways were overrepresented within strain or diet-affected phosphosites  
198 relative to all insulin-regulated sites, implying that genetics and environment modulate most or all  
199 outcomes of insulin. For instance, strain and diet affected regulatory phosphosites controlling vesicle  
200 trafficking (S348, T575, S595, and T649 on the GLUT4 trafficking regulator Tbc1d4); glucose  
201 metabolism (S469 and S486 on Pfkfb2, which promote glycolysis); mitochondrial structure and  
202 function (S129 on Mff, which promotes mitochondrial fission); autophagy (S555 on the master  
203 autophagy regulator Ulk1); gene transcription (the inhibitory site S108 on the transcription factor Tfeb);  
204 and mRNA translation (S236 on ribosomal proteins S6, S422 on Eif4b, and S64 and T69 on Eif4ebp1,  
205 which promote translation). Interestingly, Strain and Diet effects overlapped significantly (fold  
206 enrichment = 1.50,  $p = 4.40 \times 10^{-9}$ , two-sided Fisher's exact test, **Fig. S3j**), implying some phosphosites  
207 may be more amenable to regulation overall. As a notable exception, all six insulin-regulated  
208 phosphosites on Plin1 had Diet effects while only one had a Strain effect (**Fig. 3**). Plin1 coats and  
209 regulates lipid droplets, hence this enrichment of Diet effects may represent a signalling response to  
210 increased intramuscular lipids in the HFD condition. Overall, genetics and environment triggered  
211 widespread alterations in insulin signalling impinging on diverse cellular pathways.

212

213 ***Genetics and diet rewire insulin-regulated kinase signalling***

214 The extensive signalling changes caused by genetics and diet may result from altered kinase regulation.  
215 We tested this hypothesis using a kinase substrate enrichment analysis (KSEA)<sup>40</sup> on phosphopeptide  
216 insulin responses. KSEA accurately captured the activation of canonical insulin-regulated kinases (Akt,  
217 mTOR, p70S6K, and p90RSK) and the deactivation of GSK3, confirming the validity of the approach  
218 (**Fig. 4a**). Focussing on CHOW-fed mice, we identified seven kinases differentially enriched across  
219 mouse strains (ANOVA adjusted  $p$ -value  $< 0.05$ , **Fig. 4b**). For example, insulin activated SGK and  
220 deactivated GSK3 more in C57Bl6J and NOD than in other strains (**Fig. 4b**). Extending this analysis to  
221 all mice, we identified kinases with Uniform diet or StrainxDiet effects (**Fig. 4c**). Akin to our analysis

222 of individual phosphosites (**Fig. 2**), StrainxDiet effects were more prevalent than Uniform diet effects  
223 (five kinases compared to one), indicating that genetic background strongly influences the impact of  
224 HFD-feeding on kinase signalling. These results suggest that the observed phosphosite signalling  
225 changes could be partly due to altered insulin regulation of multiple kinases.

226

227 ***Biological variation reveals functional organisation of the insulin signalling network***

228 KSEA predicted changes in overall kinase activity, but we questioned if substrates of the same kinase  
229 could be differentially regulated by genetic and environmental variation. As a case study we examined  
230 substrates of Akt – a master regulator of insulin signal transduction – to assess the similarity of their  
231 insulin responses across strains and diets. Strikingly, we observed a range of both positive and negative  
232 correlations (**Fig. 5a**). For instance, while Tsc2 S939 and Akt1s1 T247 both activate mTORC1, their  
233 insulin responses correlated poorly ( $r = 0.202$ ,  $p = 0.168$ , **Fig. 5b**). Supporting these findings, similar  
234 heterogeneity in Akt substrate insulin responses has previously been observed in skeletal muscle from  
235 humans with differing metabolic health<sup>41</sup>. Hierarchical clustering revealed four distinct groups of  
236 positively correlated Akt substrates (**Fig. 5a**), suggesting these groups may coordinate distinct  
237 functional outputs of Akt signalling.

238 We next explored if the genetic and environmental variation in our study could reveal  
239 organisational principles of the entire insulin signalling pathway. By performing weighted gene  
240 correlation network analysis (WGCNA<sup>42,43</sup>), we identified eight subnetworks of coregulated insulin-  
241 responsive phosphopeptides (**Fig. 5c**) varying in size from 16 to 120 phosphopeptides, with 91 assigned  
242 to no subnetwork (**Fig. 5d**, **Table S3**). Examining the subnetwork “eigenpeptides” – a weighted average  
243 of the constituent phosphopeptides<sup>42,43</sup> – revealed that the subnetworks captured distinct effects of  
244 genetics and diet on insulin signalling (**Fig. 5e**, **Fig. S4a**). For example, HFD-feeding attenuated the  
245 insulin response of subnetwork I in CAST and C57Bl6J strains (t-test adjusted  $p = 0.0256$ ,  $0.0365$ ),  
246 while subnetwork II was affected by HFD-feeding only in CAST and NOD (**Fig. 5e**, **Fig. S4a**, t-test  
247 adjusted  $p = 0.00258$ ,  $0.0256$ ). This suggests that the subnetworks may be sensitive to distinct cellular  
248 information.

249 Next, we characterised the regulatory and functional nature of these subnetworks. Canonical  
250 insulin-regulated kinases such as Akt and mTOR were enriched across multiple subnetworks (**Fig. 5f**),  
251 confirming that genetic and environmental variation can reveal uncoupling of substrates targeted by the  
252 same kinase (**Fig. 5a-b**). Nevertheless, visualising these subnetworks within our curated insulin  
253 signalling pathway (**Fig. 3**) revealed cases where signal flowed through a single subnetwork, such as  
254 from Erk2 (Y185) to its target kinase Rsk2 (T365 and S369) and Rsk2 substrates (Gab2 S211 and Nos1  
255 S847) within subnetwork III (**Fig. S5**). Within multiply phosphorylated proteins, phosphosites either  
256 belonged to the same subnetwork (e.g. Plin1) or diverse subnetworks (e.g. Tbc1d4 and the transcription  
257 factor Nfatc2), suggesting the latter may serve as hubs integrating diverse cellular information (**Fig. S5**).

258 Some subnetworks were enriched in specific cellular compartments (GO ontologies), implying  
259 that common localisation may facilitate coregulation of phosphosites (**Fig. 5g**). Coregulation may  
260 partition functional outcomes of insulin action, as certain biological processes were enriched only in  
261 select subnetworks (**Fig. 5h**). These included known insulin targets like “negative regulation of lipid  
262 catabolic process” in subnetwork I and “positive regulation of glycogen biosynthetic process” in I, VI,  
263 and VIII (**Fig. 5h**). To further probe functional differences we analysed phosphopeptide subnetwork  
264 membership scores, which revealed additional pathways enriched in individual subnetworks. However,  
265 these results were not significant after p-value adjustment and hence are suggestive only (**Fig. S4b-d**).  
266 Lastly, we leveraged our previous phosphoproteomic time course of insulin signalling to interrogate  
267 subnetwork dynamics<sup>10</sup> and found that phosphopeptide insulin response dynamics varied across  
268 subnetworks (**Fig. 5i**). This reveals distinct temporal regulation as another feature underlying the  
269 substructure of the insulin signalling network. Overall, genetic and environmental diversity illuminated  
270 the complex coregulation structure of insulin signalling, featuring subnetworks that evade known  
271 network circuitry and present unique functional signatures.

272

### 273 ***Leveraging biological variation to identify drivers of insulin responsiveness***

274 We have so far described the marked influence of genetic background and HFD-feeding on skeletal  
275 muscle insulin signalling, evident at the level of individual phosphosites, protein kinases, and co-  
276 regulated network modules. We hypothesised that by associating this signalling diversity with a  
277 phenotypic output of insulin, such as enhanced glucose uptake, we would filter out mechanistically  
278 irrelevant phosphosites and hence prioritise molecular regulators of the phenotype. To test this  
279 hypothesis, we measured *in vivo* glucose uptake with <sup>3</sup>H-2DG tracer in the same muscle samples used  
280 for phosphoproteomics. Insulin-stimulated glucose uptake differed by more than twofold across strains  
281 (two-way ANOVA strain effect  $p = 4.78 \times 10^{-7}$ ) and was almost uniformly decreased by HFD-feeding  
282 (two-way ANOVA diet effect  $p = 1.83 \times 10^{-5}$ ) (**Fig. 6a**). This highlights that genetic background and  
283 dietary status are key determinants of insulin responsiveness.

284 To prioritise signalling nodes responsible for differences in insulin responsiveness, we correlated  
285 all insulin-regulated phosphopeptides with glucose uptake in insulin-stimulated muscles, resulting in  
286 37 significantly correlated phosphopeptides ( $r > 0.35$  or  $< -0.35$ ,  $q$ -value  $< 0.1$ , **Fig. 6b**). The most  
287 significantly correlated phosphopeptide contained T1174 and S1176 on the nitric oxide synthase Nos3.  
288 The latter serves as a positive control for our analysis, as this site is known to be phosphorylated in  
289 response to insulin to promote *in vivo* glucose uptake by vasodilation<sup>44-46</sup> (**Fig. 6c**). Other correlated  
290 phosphopeptides that could modulate insulin responsiveness include S1751 on Afdn, a phosphosite  
291 implicated in insulin action<sup>47</sup>, and S196 on the Prkag2 subunit of AMPK, a major metabolic signalling  
292 hub promoting glucose uptake<sup>48</sup> (**Fig. 6b**). These examples suggest that our analysis prioritised  
293 regulators of glucose uptake.

294 While the above analysis identified phosphosites associated with glucose uptake through their  
295 absolute abundance, we hypothesized that for some phosphosites, the magnitude of their response to  
296 insulin may be a stronger determinant of insulin action. We found that the insulin response values of 13  
297 phosphopeptides correlated with insulin-stimulated glucose uptake ( $r > 0.35$  or  $< -0.35$ ,  $q$ -value  $< 0.1$ ,  
298 **Fig. 6d**). These were largely distinct from the 37 phosphopeptides identified in our first analysis,  
299 indicating that the two approaches captured complementary information. Several of these  
300 phosphopeptides could regulate insulin-stimulated glucose uptake, such as the regulatory site S469 on  
301 the enzyme Pfkfb2 which activates glycolysis, a major pathway for glucose consumption<sup>49–51</sup> (**Fig. 6e**),  
302 and S177 on Rcsd1, which could affect GLUT4 vesicle transport via actin cytoskeleton remodelling<sup>52</sup>  
303 (**Fig. 6d**). The associations identified in these analyses could arise uniquely at the level of protein  
304 phosphorylation or could be driven by changes in total protein abundance. To assess this, we mined  
305 soleus total proteomics data from a recent study of seven CHOW and HFD-fed mouse strains, three of  
306 which were in common with this study (C57BL6J, BXH9, BXD34)<sup>18</sup>. Of the 34 glucose uptake-  
307 associated phosphoproteins we identified, 16 were quantified in both studies and only two additionally  
308 correlate with glucose uptake at the total protein level (Ppp6rl and Ttn, **Fig. S6a**). Hence, it seems  
309 likely that most glucose uptake-phosphosite associations were not driven by protein abundance changes,  
310 underscoring the utility of phosphoproteomics to provide unique information on top of more classical  
311 omics layers.

312 In addition to individual phosphosites, the status of larger signalling network components could  
313 also influence insulin responsiveness. Kinase enrichment scores affected by strain or diet did not  
314 correlate with glucose uptake (**Table S4**), suggesting insulin action is not dominated by the net activity  
315 of specific kinases. Interestingly, two WGCNA-derived insulin signalling subnetworks correlated with  
316 glucose uptake: subnetwork V ( $r = 0.436$ ,  $p = 0.00173$ ) and subnetwork I ( $r = 0.332$ ,  $p = 0.0197$ , **Fig.**  
317 **6f**). Subnetwork V could modulate glucose uptake through actin cytoskeleton remodelling via Rscd1  
318 S177, through glucose metabolism promotion via Gys1 S641 (**Table S3**), and by influencing GLUT4  
319 vesicle trafficking due to its enrichment at “cytoplasmic vesicle membranes” (**Fig. 5g**). It was also  
320 enriched in substrates of GSK3, which has been implicated in insulin resistance in skeletal muscle<sup>53–55</sup>  
321 and adipose tissue<sup>32</sup>. Subnetwork I, the largest cluster containing 27% of insulin-regulated  
322 phosphopeptides, was enriched in multiple kinases and biological processes (**Fig. 5f, h**), suggesting it  
323 may be a central regulatory hub for various outcomes of insulin action including glucose uptake.  
324 Examining the subnetwork membership scores for glucose-uptake correlated phosphopeptides also  
325 revealed a preference for clusters V and I, supporting this analysis (**Fig. S6b-c**). Overall,  
326 compartmentalisation of insulin-responsive phosphosites into subnetworks may enable independent  
327 control of insulin’s functional outputs, since only two subnetworks correlated with insulin-stimulated  
328 glucose uptake.

329

330

331 ***Upregulating glycolysis reverses insulin resistance***

332 We next aimed to validate our approach for identifying regulatory mechanisms of insulin-stimulated  
333 glucose uptake. S469 on Pfkfb2 correlated highly with glucose uptake follow insulin stimulation (**Fig.**  
334 **6e**). Phosphorylation of this site leads to increased production of F2,6BP, a potent glycolytic agonist,  
335 suggesting that activating glycolysis may play a key role in muscle insulin responsiveness. This is  
336 consistent with our previous findings that glycolytic enzyme abundance was strongly associated with  
337 *ex vivo* insulin-stimulated glucose uptake in muscle from inbred mice<sup>18</sup>, that the insulin resistance-  
338 reversing small molecule thiostrepton enhances glycolytic capacity<sup>56</sup>, and that decreasing glycolytic  
339 flux caused insulin resistance *in vitro*<sup>57</sup>. To further establish glycolysis as a regulator of insulin  
340 responsiveness in skeletal muscle, we decided to investigate whether upregulating glycolysis through  
341 F2,6BP production can restore insulin-stimulated glucose uptake in insulin resistance.

342 Since Pfkfb2 requires phosphorylation by Akt to produce F2,6BP substantially, increasing  
343 F2,6BP production via Pfkfb2 would require enhanced activating site phosphorylation, which is  
344 difficult to achieve in a targeted fashion, or phosphomimetic mutation of activating sites to  
345 aspartate/glutamate, which often does not recapitulate the molecular effects of serine/threonine  
346 phosphorylation<sup>58</sup>. By contrast, the paralog Pfkfb3 has high basal production rates and lacks an Akt  
347 motif at the corresponding phosphosites<sup>51</sup>. We therefore rationalised that overexpressing Pfkfb3 would  
348 robustly increase F2,6BP production and enhance glycolysis regardless of insulin stimulation and Akt  
349 signalling (**Fig. 6g**). To avoid systemic effects of Pfkfb3 overexpression we studied cultured L6-  
350 GLUT4-HA myotubes, which display robust insulin regulation of GLUT4 trafficking and develop  
351 insulin resistance upon palmitate treatment, mimicking lipotoxicity, a trigger of *in vivo* insulin  
352 resistance<sup>59</sup>. While L6 cells are of rat origin, they are preferable to the popular C2C12 mouse cell line  
353 since the latter lack an insulin-responsive vesicular compartment<sup>60</sup> and undergo spontaneous contraction,  
354 resulting in confounding non-insulin dependent glucose uptake<sup>61</sup>.

355 As anticipated, Pfkfb3 overexpression increased glycolytic capacity in L6-GLUT4-HA myotubes  
356 as measured by extracellular acidification rate (**Fig. S7a-c**). Pfkfb3 overexpression also restored insulin-  
357 responsive glucose uptake to normal levels in palmitate-treated cells (**Fig. 6h**, **Fig. S7d**). This effect  
358 was only observed in cells treated with palmitate and insulin, suggesting it specifically modulated  
359 insulin action rather than non-specifically increasing glucose uptake through enhanced glucose  
360 consumption (**Fig. S7d**). This may be due to enhanced insulin signalling, as we have previously  
361 observed that transient Pfkfb3 overexpression increased Akt signalling in HEK293 cells<sup>57</sup>. However,  
362 immunoblotting of canonical insulin-responsive phosphosites on Akt and its substrates GSK3α/β and  
363 PRAS40 revealed minimal effect of palmitate treatment and Pfkfb3 overexpression (**Fig. S7e-f**), hence  
364 more detailed phosphoproteomics studies are needed to clarify whether Pfkfb3 overexpression restored  
365 insulin action by modulating insulin signalling. Overall, our results further establish glycolytic flux as  
366 a major determinant of the glucose uptake arm of muscle insulin action and highlight the power of  
367 studying phosphoproteomics across the gene-by-environment landscape to identify causal drivers of

368 complex phenotypes. We anticipate that our catalogue of glucose uptake-correlated phosphosites will  
369 provide a rich starting point for future investigations into mechanisms of insulin action and resistance.

370 **Discussion**

371 The environment shapes the flow of information from genotype to phenotype. Many studies have  
372 interrogated the role of intermediate molecular layers such as the transcriptome or proteome, however  
373 few studies have examined how protein post-translation modifications participate in this information  
374 transfer. Here we have approached this problem by leveraging diverse inbred mouse strains and  
375 phosphoproteomics to examine the insulin signalling network across a landscape of genetic and dietary  
376 variation. Genetic background significantly altered the insulin signalling network both independently  
377 and in concert with dietary status, affecting myriad phosphosites and multiple kinases. We exploited  
378 this variation in signalling responses in two ways – to study the partitioning of the Akt and insulin  
379 signalling pathways into distinct subnetworks of coregulated phosphosites; and to identify potential  
380 regulators of insulin responsiveness by associating phosphorylation with insulin-stimulated glucose  
381 uptake. Finally, validation studies in L6 myotubes confirmed the major role of accelerated glycolysis  
382 as a key regulator of insulin responsiveness.

383 Genetic and diet-driven signalling changes did not transmit linearly through our current model  
384 of the insulin signalling network, illustrating that this model remains incomplete. Notably, substrates of  
385 kinases such as Akt clustered into distinct groups based on differing insulin responses. Hence, it is an  
386 oversimplification to model signalling pathways as networks of individual kinases since substrates of  
387 the same kinase display independent regulation. This could arise from localisation of a kinase to distinct  
388 substrate pools<sup>62–64</sup>; interactors targeting a kinase to different substrates<sup>62</sup>; substrate phosphorylation by  
389 alternate kinases<sup>65</sup>; the dephosphorylation of specific substrates by phosphatases; kinase post-  
390 translational modifications altering substrate specificity; and distinct substrate phosphorylation  
391 kinetics<sup>10</sup>. As our knowledge of the repertoire of kinase substrates continues to deepen<sup>66</sup>, future research  
392 should explore how the above mechanisms contribute to finer regulation of these substrates. Genetic  
393 and environmental variation also exposed a coregulation subnetwork structure within the insulin  
394 signalling network. The enrichment of subnetworks in distinct biological processes, and the selective  
395 association of two subnetworks with glucose uptake, suggests that this coregulation structure may direct  
396 independent control of distinct outcomes of insulin action. This exciting possibility necessitates further  
397 investigation, including replication in independent cohorts and spatiotemporal characterisation of  
398 subnetwork dynamics. Alternatively, one could overlap subnetworks with genetic information, such as  
399 genes associated with glucose homeostasis and other metabolic traits in human GWAS studies<sup>67</sup>, or  
400 muscle-specific eQTLs or pQTLs genetically colocalised with similar traits<sup>68</sup>, to further prioritise  
401 subnetwork-associated phenotypes and identify potential drivers within subnetworks.

402 Muscle insulin signalling responses vary across individuals<sup>22,41</sup>, and our results suggest that  
403 baseline genetic differences and an individual's environment both alter signalling, with the  
404 environment's influence depending strongly on genetic background. Signalling pathways are popular  
405 therapeutic targets due to their importance in human health and the relative ease of pharmaceutical  
406 interventions<sup>69</sup>. Our results advocate for a personalised approach to such therapies, implying that the

407 efficacy of treatments aiming to correct pathological signalling responses will depend on an individual's  
408 genetic background. In cancer, where signalling networks are dysregulated heterogeneously, modelling  
409 patient-specific networks has already shown promise for identifying personalised drug targets<sup>70,71</sup>.  
410 Personalised medicine approaches will also be aided by a comprehensive understanding of how genetics  
411 shape signalling networks and potentiate their modulation by the environment. Recent studies have  
412 made the first step, revealing that the ground-state phosphoproteome can be altered by mutations  
413 affecting network components such as kinases, phosphatases, and phosphoproteins, as well as the  
414 molecular milieu the network is exposed to including extracellular signalling ligands<sup>20,21</sup>. An important  
415 corollary of such genetic factors is that multiple genetic backgrounds should be studied when  
416 establishing generalizable signalling responses. Our data indicate that insulin responses in C57BL6J –  
417 the most commonly studied mouse strain – are not necessarily generalizable, indicated by phosphosites  
418 such as S15 on Rnmt that were insulin regulated almost exclusively in C57Bl6J.

419 A major challenge in studying signal transduction with omics technologies is that hundreds to  
420 thousands of molecular events typically respond to a cellular signal, making it difficult to pinpoint the  
421 most crucial regulatory nodes. To tackle this challenge, we previously demonstrated that associating  
422 phosphoproteomics with physiological phenotypes across diverse individuals enriches for phosphosites  
423 more likely to modulate biological responses<sup>22</sup>. Here we have elaborated on this approach, revealing  
424 that associating phosphorylation with phenotype across a genetic and environmental landscape can  
425 identify regulators of specific biological processes, such as insulin-stimulated glucose uptake. Our  
426 results recapitulated known glucose uptake regulators and led to further validation of glycolytic flux as  
427 a modulator of insulin responsiveness. We have previously demonstrated that reduced glycolytic flux  
428 impairs GLUT4 translocation and insulin signalling<sup>57</sup>, implying that the status of glycolysis is sensed  
429 by proteins regulating insulin action. An enhanced glycolytic metabolic tone may alter production of  
430 reactive oxygen species, a known modulator of insulin action<sup>59,72,73</sup> and insulin signalling<sup>74</sup>.  
431 Alternatively, recent approaches to map protein-metabolite interactions could identify points of  
432 allosteric crosstalk between glycolytic metabolites and insulin action proteins<sup>75,76</sup>, hence broadening our  
433 understanding of the bidirectional communication between insulin action and metabolism.

434 It was striking that only several dozen insulin-regulated phosphopeptides associated significantly  
435 with glucose uptake. Since insulin triggers multiple distinct cellular outcomes, it is possible that only a  
436 subset of insulin-responsive phosphosites contribute to enhanced glucose uptake. Moreover, many of  
437 these phosphosites might only be permissive for insulin-stimulated glucose uptake and are not major  
438 regulatory nodes determining the fidelity of the process. For example, while mutation of the four  
439 primary Akt regulatory sites on Tbc1d4 blocks GLUT4 translocation<sup>77</sup>, none of these phosphosites  
440 featured strong positive correlations with glucose uptake in our analysis (**Fig. S8**). This implies that  
441 their phosphorylation may promote glucose uptake in a functionally permissive, switch-like fashion.  
442 We suggest that the glucose uptake-associated phosphosites we have identified will be enriched in major

443 regulators of insulin responsiveness, necessitating future functional studies to characterise these sites  
444 and explore their involvement in insulin resistance.

445 Our work demonstrates that genetic and environmental variation can profoundly modulate global  
446 signalling networks and that the influences of these factors are intrinsically entwined. We show that the  
447 resulting diversity in signalling responses can be leveraged to pinpoint regulators of insulin-stimulated  
448 glucose uptake, providing a powerful methodological framework for interrogating the regulatory basis  
449 of complex biological pathways.

450

451 ***Limitations of this study***

452 First, this study focused on male mice and examined only five inbred strains. This limited number of  
453 strains may mean that our association analysis was underpowered to detect some regulators of insulin  
454 responsiveness. Importantly, however, this does not imply that the regulators identified are incorrect,  
455 but only that there may be more to discover with larger cohorts. In addition, studies incorporating male  
456 and female subjects found that mouse insulin sensitivity was affected by interactions between sex and  
457 strain<sup>78</sup>, and insulin signalling in stem cell-derived myoblasts by interactions between sex and donor  
458 metabolic health<sup>31</sup>. Hence, we anticipate that sex would contribute another important dimension to the  
459 web of interactions between genetics, diet, and insulin signalling identified here. Future work should  
460 therefore extend our approach across a broader range of genetic backgrounds, as well as in female mice.  
461 Second, we only examined insulin signalling after 10 minutes, since measuring multiple timepoints  
462 would have drastically increased the number of animals and samples required. Integration of dynamic  
463 phosphoproteome data from cultured cells indicated that insulin signalling dynamics may contribute to  
464 trends in our data (Fig. 5i), suggesting the exploration of signalling at additional timepoints may be  
465 fruitful in the future.

466 Third, mammalian tissues are a heterogeneous mixture of cell types, and differences in this  
467 mixture could result in different signalling responses measured at the whole tissue level. In our  
468 experience, the soleus can be reproducibly dissected as an intact muscle with little contamination from  
469 surrounding tissues, making it unlikely that cell type composition varied across samples due to tissue  
470 collection. However, we cannot exclude the possibility that differences in the composition of the soleus  
471 muscle across strains and diets contributed to the signalling changes we detected. We were also unable  
472 to determine the extent to which signalling changes arose from muscle-intrinsic or extrinsic factors. For  
473 instance, body weight varied substantially across mice and correlated significantly with 25% of Strain  
474 and Diet-affected phosphopeptides (Fig. S8c), suggesting obesity-related systemic factors likely impact  
475 a subset of the muscle insulin signalling network. Furthermore, genetic differences in lifespan could  
476 alter the “biological age” of different strains and their phosphoproteomes, though we could not assess  
477 this possibility since lifespan data is not available for most strains used. Lastly, as we did not perform  
478 total proteomics, we did not assess whether phosphosite changes were caused by differences in total  
479 protein abundance. However, since protein abundance should not change within a 10-minute insulin

480 stimulation<sup>32</sup>, the acute insulin responses we observed should only reflect differences in protein  
481 phosphorylation. Furthermore, in our previous studies of insulin signalling in adipocytes<sup>32</sup> or human  
482 skeletal muscle<sup>22</sup> in which deep proteomes were measured in parallel, we found little global correlation  
483 between changes in protein phosphorylation and protein abundance across experimental conditions  
484 regardless of insulin stimulation, suggesting the contribution of protein abundance to phosphosite  
485 changes across strains and diets was likely minimal.

486

487

#### 488 **Additional information**

##### 489 **Acknowledgements**

490 D.E.J. is an Australian Research Council (ARC) Laureate Fellow. The content is solely the  
491 responsibility of the authors and does not necessarily represent the official views of the ARC. The  
492 authors also acknowledge the facilities, and the scientific and technical assistance of the Sydney Mass  
493 Spectrometry Facility and the Laboratory Animal Services at the Charles Perkins Centre, University of  
494 Sydney.

495

##### 496 **Author Contributions**

497 Conceptualization: JvG, SWCM, SJH, DEJ. Methodology: JvG, HBC, SWCM, ADV, MP, SJH. Formal  
498 analysis: JvG. Investigation: JvG, SWCM, HBC, ADV, MP, JS, SM, MEN, SJH. Resources: JS.  
499 Writing – Original Draft: JvG. Writing – Review and Editing: All authors. Visualization: JvG.  
500 Supervision: SWCM, SJH, DEJ. Project Administration: JvG, SWCM, SJH, DEJ. Funding Acquisition:  
501 DEJ

502

##### 503 **Declaration of Interests**

504 The authors declare no competing interests.

505

##### 506 **Data Access Statement**

507 All raw and Spectronaut processed phosphoproteomics data have been deposited in the PRIDE  
508 proteomeXchange repository and will be made publicly available upon publication. Processed data are  
509 available as supplementary tables.

510

##### 511 **Code availability**

512 All code used to analyse data and produce figures has been uploaded to  
513 [https://github.com/JulianvanGerwen/GxE\\_muscle\\_phos](https://github.com/JulianvanGerwen/GxE_muscle_phos)

514

##### 515 **Methods**

##### 516 **Statistical analysis**

517 Most statistical analysis was performed in the R programming environment using RStudio (R version:  
518 4.2.1, RStudio version: 2022.07.1 Build 554). Analysis of GLUT4-HA-L6 myotube Pfkfb3 expression,  
519 2DG uptake, and ECAR was performed in GraphPad Prism (version: 9.3.1).

520

### 521 ***Animal details***

522 Male C57BL/6J (C57Bl6J), BXH9/TyJ (BXH9), BXD34/TyJ (BXD34), and CAST/EiJ (CAST) mice  
523 were purchased from Australian BioResources (Moss Vale, NSW, Australia) while NOD/ShiLtJ (NOD)  
524 mice were purchased from Animal Resources Centre (Murdoch, WA, Australia). Mice were at most 9  
525 weeks old upon arrival. Mice were housed at 23 °C on a 12 h light/dark cycle in cages of 2-5, with free  
526 access to food and water. At 12-16 weeks of age mice were randomly allocated to a standard CHOW  
527 diet (13% calories from fat, 65% from carbohydrate, 22% from protein; “Irradiated Rat and Mouse  
528 Diet”, Specialty Feeds, Glen Forrest, WA, Australia) or a high-fat high-sucrose diet made in house  
529 (HFD; 45% calories from fat (40% calories from lard), 35% from carbohydrate (14% calories from  
530 starch), and 22% from protein) and sacrificed exactly 6 weeks later. The number of mice in each group  
531 are C57Bl6J: 8 CHOW, 10 HFD; NOD: 10 CHOW, 10 HFD; BXH9: 8 CHOW, 9 HFD; CAST: 9  
532 CHOW, 9 HFD; BXD34: 10 CHOW, 11 HFD. Procedures were carried out with approval from the  
533 University of Sydney Animal Ethics Committee following guidelines issued by NHMRC (Australia).

534

### 535 ***Assessment of body composition***

536 Body composition of individual mice was assessed using the EchoMRI-900 to determine lean mass 1  
537 day before a glucose tolerance test and 5-6 days before euthanasia. Analysis was performed as per the  
538 manufacturer’s specifications.

539

### 540 ***Glucose tolerance test***

541 On the day of a glucose tolerance test mice were fasted for 6 h (0800-1400). Mice were then orally  
542 gavaged with 20% (w/v) glucose in water at 2 g/kg lean mass, and blood glucose was measured from  
543 the tail vein using a glucometer 0, 15, 30, 45, 60, and 90 min after the gavage. At 0 and 15 min, 5 µL  
544 blood was also collected into an Insulin Mouse Ultra-Sensitive ELISA plate (Crystal Chem USA, Elk  
545 Grove Village, Illinois, USA). Blood insulin concentration was measured according to the  
546 manufacturer’s protocol, using linear extrapolation from an insulin standard curve. The area of the blood  
547 glucose curve (AOC) was calculated by:

$$548 AOC = \sum_{i=2}^n \frac{(G_{i-1} - G_1) + (G_i - G_1)}{2} (t_i - t_{i-1})$$

549 Where  $i$  represents the  $i^{\text{th}}$  timepoint at which blood glucose was measured,  $n$  represents the last  
550 timepoint,  $t_i$  represents the time (min) of the  $i^{\text{th}}$  timepoint, and  $G_i$  represents blood glucose  
551 concentration (mM) at the  $i^{\text{th}}$  timepoint.

552

553 ***In vivo insulin stimulation***

554 On the day of the procedure mice were fasted for 2h (1100-1300). Mice were then anaesthetised by  
555 intraperitoneal injection of sodium pentobarbital at 80 mg/kg body mass. To counter anaesthesia-  
556 associated declines in body temperature, mice were wrapped in aluminium foil and placed on a heating  
557 pad at 37°C. After 15 min anaesthesia, mice were injected retro-orbitally as previously described<sup>79</sup> with  
558 50 µL plasma replacement (B. Braun, Melsungen, DEU) containing 10 µCi <sup>3</sup>H-2DG and saline or  
559 insulin (0.75 U/kg lean mass). Blood glucose was measured from the tail vein using a glucometer  
560 (AccuCheck, Roche Diabetes Care, NSW, Australia) 1 min prior to injection and 1, 5, 7.5, and 10 min  
561 after injection. Simultaneously, 5 µL blood was collected into 95 µL 0.9% NaCl on ice to measure <sup>3</sup>H-  
562 2DG blood concentration. Ten minutes after insulin injection mice were sacrificed by cervical  
563 dislocation and the soleus muscle was rapidly excised, immediately frozen in liquid nitrogen, and stored  
564 at -80°C. To measure <sup>3</sup>H-2DG blood concentration, diluted blood samples were first centrifuged at  
565 10,000 xg for 10 min to pellet blood cells. Supernatant (70 µL) was collected and combined with 3 mL  
566 liquid scintillation cocktail (Perkin Elmer, Massachusetts, USA: 6013321) to allow the measurement of  
567 <sup>3</sup>H with a Tri-Carb 2810TR Liquid Scintillation Counter (Perkin Elmer, Massachusetts, USA).

568

569 ***Skeletal muscle lysis***

570 Frozen muscle tissue was powdered by grinding in a mortar and pestle chilled with liquid nitrogen and  
571 dry ice. To lyse powdered tissue, 200 µL lysis buffer (4% (w/v) sodium deoxycholate, 100 mM Tris-  
572 HCl pH 8.5) was added followed by 10 s vortexing. Samples were then sonicated at 4 °C at 90% power  
573 using pulses of 2 s on, 5 s off for a total time of 1 min. Samples were then immediately boiled at 95 °C  
574 with 1,500 rpm shaking for 5 min and sonicated for a further 2 min (4 °C, 90% power, 5 s on and 5 s  
575 off) to ensure complete lysis. Lysate was then centrifuged at 20,000 xg for 5 min and 180 µL supernatant  
576 was collected. Cysteine residues were reduced and alkylated by adding 40 mM chloroacetamide and 10  
577 mM TCEP at pH 7. Lysate was incubated for 5 min at 45 °C with 1,500 rpm shaking and then incubated  
578 for a further 40 min at room temperature without shaking.

579 Next, 800 µL 100% chloroform and 1,600 µL 100% methanol were added following 30 s  
580 sonication at 90% power. LC/MS grade water (800 µL) was added following 5 min mixing at 1,000  
581 rpm. Lysate was centrifuged for 5 min at 2,000 xg to induce a phase separation. The majority of the  
582 aqueous phase (2,400 µL) was removed and 2,000 µL was reserved for <sup>3</sup>H-2DG quantification. Next,  
583 2,400 µL 100% methanol was added following 30 s mixing at 800 rpm and centrifugation at 2,000 xg  
584 for 5 min. The supernatant was discarded, and the protein pellet was air-dried for 5 min. Protein was  
585 reconstituted in 200 µL lysis buffer, sonicated at 60% power for 15 s using a tip-probe sonicator and  
586 boiled for 5 min in a thermomixer at 95 °C with 1,500 rpm shaking.

587

588 ***Determining <sup>3</sup>H-2DG uptake into muscle tissue***

589 Anion exchange chromatography was used to quantify  $^3\text{H}$ -p2DG, representing  $^3\text{H}$ -2DG that has been  
590 taken up by cells. For quantification of total (phosphorylated and unphosphorylated)  $^3\text{H}$ -2DG, 375  $\mu\text{L}$   
591 lysate aqueous phase was combined with 1,125  $\mu\text{L}$  water and reserved. For quantification of  
592 unphosphorylated  $^3\text{H}$ -2DG, 1,000  $\mu\text{L}$  lysate aqueous phase was added to 300  $\mu\text{L}$  37.5% (w/v) AG 1-  
593 X8 anion exchange resin (Bio-Rad, Hercules, CA, USA: 1401441) and washed with 3 mL water to  
594 remove p2DG. Liquid scintillation cocktail (3 mL) was then added to 1,500  $\mu\text{L}$  total and  
595 unphosphorylated  $^3\text{H}$ -2DG solutions, and  $^3\text{H}$ -2DG was measured using a Tri-Carb 2810R Liquid  
596 Scintillation Counter. Unphosphorylated and total  $^3\text{H}$ -2DG scintillation counts were subtracted to  
597 quantify  $^3\text{H}$ -p2DG.

598  $^3\text{H}$ -2DG blood concentration at 1, 5, 7.5, and 10 min after injection was fit to an exponential  
599 curve  $y = C_p(0)e^{-K_p t}$  where  $C_p(0)$  represents the predicted initial tracer concentration (DPM/ $\mu\text{L}$ ) and  
600  $K_p$  represents the rate of tracer disappearance from the blood (1/min), to model the disappearance of  
601  $^3\text{H}$ -2DG from the blood as it is taken up and trapped by peripheral tissues<sup>80</sup>.  $C_p(1)$  was removed when  
602 it was abnormally low ( $C_p(1) < C_p(5)$ ,  $C_p(5) - C_p(1) > 0.5 \times (C_p(5) - C_p(7.5))$ ), which likely  
603 indicates insufficient diffusion of circulating  $^3\text{H}$ -2DG into the tail vein. To account for different rates  
604 of blood  $^3\text{H}$ -2DG disappearance across mice,  $^3\text{H}$ -2DG uptake was calculated as a rate constant<sup>80</sup>:

$$605 K_i = \frac{C_i(t)K_p}{C_p(0)(1 - e^{-K_p t})}$$

606 Where  $t$  represents the time after injection that the animal was sacrificed (min) and  $C_i(t)$  represents the  
607 concentration of  $^3\text{H}$ -p2DG in the tissue harvested at time  $t$  (DPM/mg tissue).

608

### 609 *Phosphoproteomics sample preparation*

610 Phosphopeptides were isolated using the EasyPhos protocol<sup>28</sup> with minor modifications. Protein  
611 (C57Bl6J and NOD: 755  $\mu\text{g}$ , BXH9 and BXD34: 511  $\mu\text{g}$ , CAST: 364  $\mu\text{g}$ ) was digested into peptides  
612 by incubation in 1% (w/w) Trypsin and LysC on a thermomixer at 37°C with 1,500 rpm shaking for 14  
613 h. Following digestion, 400  $\mu\text{L}$  100% isopropanol and 100  $\mu\text{L}$  EasyPhos enrichment buffer (48% (v/v)  
614 TFA, 8 mM KH<sub>2</sub>PO<sub>4</sub>) were sequentially added with mixing (1,500 rpm, 30 s) after each addition. Lysate  
615 was centrifuged at 20,000 xg for 15 min to pellet insoluble material and transferred to a deep well plate.  
616 The EasyPhos protocol was then followed from step 12<sup>28</sup>.

617

### 618 *Liquid chromatography-tandem mass spectrometry (LC-MS/MS)*

619 Enriched phosphopeptides in MS loading buffer (2% ACN, 0.3% TFA) were loaded onto in-house  
620 fabricated 55 cm columns (75  $\mu\text{M}$  I.D.), packed with 1.9  $\mu\text{M}$  C18 ReproSil Pur AQ particles (Dr.  
621 Maisch HPLC GmbH, Ammerbuch, DEU) with a Dionex U3000 HPLC (Thermo Fisher Scientific),  
622 interfaced with an Orbitrap Exploris 480 mass spectrometer (Thermo Fisher Scientific). Column  
623 temperature was maintained at 60°C using a column oven (Sonation lab solutions, Biberach, DEU), and  
624 peptides were separated using a binary buffer system comprising 0.1% formic acid (buffer A) and 80%

625 ACN plus 0.1% formic acid (buffer B) at a flow rate of 400 nL/min. A gradient of 3–19% buffer B was  
626 employed over 40 min followed by 19–41% buffer B over 20 min, resulting in approximately 1 h  
627 gradients. Peptides were analysed with one full scan (350–1,400 m/z, R = 120,000) at a target of 3e<sup>6</sup>  
628 ions, followed by 48 data-independent acquisition MS/MS scans (350–1,022 m/z) with higher-energy  
629 collisional dissociation (target 3e<sup>6</sup> ions, max injection time 22 ms, isolation window 14 m/z, 1 m/z  
630 window overlap, normalised collision energy 25%), and fragments were detected in the Orbitrap (R =  
631 15,000).

632

633 ***MS raw data processing***

634 Raw spectral data were analysed using Spectronaut (v16.0.220606.53000). Data were searched using  
635 directDIA against the Mouse UniProt Reference Proteome database (January 2022 release), with default  
636 settings (precursor and protein Qvalue cutoffs 0.01, Qvalue filtering, MS2 quantification), with “PTM  
637 localization” filtering turned on (threshold 0.5), and the inbuilt peptide collapse function.

638

639

640 ***Phosphoproteomics data processing***

641 Phosphopeptide intensities were log2 transformed and median normalised. Non-class I phosphopeptides  
642 (localisation score  $\leq 0.75$ ) were then removed. Finally, for each phosphopeptide, outlier values were  
643 removed that had a log2 intensity  $< 5$  and were  $> 6$  log2 intensity units lower than the phosphopeptide  
644 median. Log2 fold changes between conditions were computed using condition medians.

645

646 ***Identifying insulin-regulated phosphopeptides***

647 To allow comparison across conditions, phosphopeptides were filtered for those highly quantified in  
648 most strain-diet combinations. For a given phosphopeptide, this filtering was performed on two levels.  
649 Firstly, each of the 10 strain-diet combinations were retained if there were  $\geq 3$  insulin-stimulated values  
650 and  $\geq 3$  unstimulated values. Then, the phosphopeptide itself was retained if  $\geq 8$  strain-diet combinations  
651 had passed the previously filtering. Phosphopeptides were then fit to a three-way ANOVA with all  
652 interaction terms (“aov” in the R package “stats”) and an F-test was performed assessing the main effect  
653 of insulin stimulation. To correct for multiple hypothesis testing p-values were converted into q-values  
654 (R package “qvalue”<sup>81</sup>). The log2(insulin/unstimulated) fold change with the greatest magnitude across  
655 strain-diet combinations was then calculated (max log2(insulin/unstimulated)). Phosphopeptides were  
656 considered “insulin-regulated” when  $q < 0.05$  and if insulin increased or decreased phosphorylation by  $>$   
657 1.5-fold in at least one strain-diet combination (max log2(insulin/unstimulated)  $> 0.58$  or  $< -0.58$ ).  
658

659

659 ***Calculation of insulin response values***

660 For all phosphopeptides the distribution of “insulin responses” in each strain-diet combination was  
661 calculated. Specifically, within each strain-diet combination all insulin-stimulated values were  
662 normalised by subtracting the unstimulated median.

663

664 ***Identifying strain and diet effects***

665 *Strain effects*

666 For each insulin-regulated phosphopeptide a one-way ANOVA was performed modelling the insulin  
667 response as a function of mouse strain within the CHOW diet. p-values were converted to q-values.  
668 For significant phosphopeptides ( $q < 0.05$ ), t-tests were performed comparing the insulin response of  
669 C57Bl6J to each of the other four strains. t-test p-values were converted to q-values and considered  
670 significant when  $q < 0.05$ . To ensure that significant differences between a strain and C57Bl6J were  
671 of a meaningful magnitude, the strain’s log2(insulin/unstimulated) was compared to the C57Bl6J  
672 log2(insulin/unstimulated). In general, if the absolute difference between the two was greater than  
673 0.58 this was accepted. However, this threshold was decreased for phosphopeptides with weaker  
674 insulin regulation. Specifically, the difference was retained if it passed the following filtering:  
675

*Strain log2(insulin/unstimulated) > f(C57Bl6J log2(insulin/unstimulated))*

or

*Strain log2(insulin/unstimulated) < g(C57Bl6J log2(insulin/unstimulated)),*  
where  $f(x)$  and  $g(x)$  are defined as:

$$f(x) = \begin{cases} x + 0.58, & \text{if } x \geq 2 \times 0.58 \\ \frac{5}{4}x + \frac{1}{2} \times 0.58, & \text{if } 0 \leq x < 2 \times 0.58 \\ x + \frac{1}{2} \times 0.58, & \text{if } -\frac{1}{2} \times 0.58 \leq x < 0 \\ \frac{4}{5}x + \frac{2}{5} \times 0.58, & \text{if } -3 \times 0.58 \leq x < -\frac{1}{2} \times 0.58 \\ x + 0.58, & \text{if } x < -3 \times 0.58 \end{cases}$$
$$g(x) = \begin{cases} x - 0.58, & \text{if } x \geq 3 \times 0.58 \\ \frac{4}{5}x - \frac{2}{5} \times 0.58, & \text{if } \frac{1}{2} \times 0.58 \leq x < 3 \times 0.58 \\ x - \frac{1}{2} \times 0.58, & \text{if } 0 \leq x < \frac{1}{2} \times 0.58 \\ \frac{5}{4}x - \frac{1}{2} \times 0.58, & \text{if } -2 \times 0.58 \leq x < 0 \\ x - 0.58, & \text{if } x < -2 \times 0.58 \end{cases}$$

676

677 An insulin-regulated phosphopeptide was considered to have a “Strain effect” if the insulin response in  
678 at least one strain was different to C57Bl6J using the q-value and log2 fold-change criteria described  
679 above.

680

#### 681 *Uniform diet and StrainxDiet effects*

682 For each insulin-regulated phosphopeptide a two-way ANOVA was performed modelling the insulin  
683 response as a function of strain, diet, and their interaction. The p-values for the Diet and StrainxDiet  
684 terms were converted to q-values. Whenever the StrainxDiet term was significant ( $q < 0.05$ ),  
685 additional tests were performed to identify specific strains in which the insulin response differed  
686 between CHOW and HFD. If the StrainxDiet term was not significant but the Diet term was  
687 significant, a separate filtering procedure was performed.

688 When the StrainxDiet term was significant, t-tests were performed to compare the CHOW  
689 insulin response to the HFD insulin response within each strain. When a t-test was significant ( $q <$   
690 0.05), the  $\log_2(\text{insulin/unstimulated})$  filtering procedure described for “Strain effects” was applied  
691 comparing CHOW and HFD fold changes. Insulin-regulated phosphopeptides were considered to  
692 have a “StrainxDiet effect” if there was a difference between CHOW and HFD in at least one strain.

693 When only the Diet term was significant, the  $\log_2(\text{insulin/unstimulated})$  filtering procedure  
694 described for “Strain effects” was applied, comparing the mean  $\log_2(\text{insulin/unstimulated})$  across  
695 strains within CHOW, to the mean across HFD. Insulin-regulated phosphopeptides that passed this filter  
696 were considered to have a “Uniform diet effect”.

697

698

699 ***Curated insulin signalling subnetwork***

700 A subnetwork of insulin-regulated phosphosites was curated by compiling all sites on proteins from a  
701 previously published knowledge pathway-derived list of canonical insulin signalling proteins<sup>22</sup>. Several  
702 phosphosites and proteins that were not detected as insulin regulated were included due to their  
703 importance in the insulin signalling pathway. Additionally, all *in vivo* substrates of canonical insulin-  
704 regulated kinases (Akt, mTOR, AMPK, Raf, Mek1/2, Erk1/2, p90RSK/Rsk2, p70S6K, Pdk1, INSR)  
705 annotated in PhosphositePlus were included<sup>33</sup>. Annotations from orthologous phosphosites were pooled  
706 across species using PhosphositePlus Site Group IDs. Phosphosite regulatory roles from  
707 PhosphositePlus were indicated after manual validation by literature search. Proteins were assigned to  
708 functional groups (e.g. mRNA processing, lipid metabolism) based on their Uniprot descriptions.

709

710 ***Kinase substrate enrichment analysis***

711 Kinase-substrate annotations were collated from PhosphositePlus and mapped into phosphoproteomics  
712 data using Site Group IDs. Only annotations supported by *in vivo* evidence were used. Annotations for  
713 kinase isoforms (e.g. Akt1, Akt2, Akt3) were merged. Substrate annotations for GSK3 were  
714 supplemented with a recent list of 274 putative GSK3 substrates determined by phosphoproteomics and  
715 motif analysis<sup>32</sup>. Autophosphorylation sites and promiscuous phosphosites targeted by  $\geq 4$  kinases were  
716 removed. Kinase substrate enrichment analysis (KSEA) was then performed with the “ksea” function  
717 from the R package “ksea”<sup>40</sup> (version: 0.1.2) using insulin response data and 1,000 permutations to  
718 determine empirical p-values. Only phosphopeptides quantified in  $\geq 50\%$  of samples and with  $\geq 1$   
719 insulin response value in all strain-diet combinations were used. In each sample kinases with  $< 5$   
720 quantified substrates were excluded, and only kinases with significant enrichment ( $p < 0.05$ ) in  $\geq 5$   
721 samples were used in subsequent analysis. To identify Strain effects on kinase activity, one-way  
722 ANOVAs were performed on CHOW KSEA enrichment scores. To identify Uniform diet or  
723 StrainxDiet effects, two-way ANOVAs were performed on KSEA enrichment scores testing the effects  
724 of strain, diet, and their interaction. p-values were adjusted by the Benjamini-Hochberg procedure.

725

726 ***Insulin signalling subnetwork analysis***

727 Weighted gene correlation network analysis (WGCNA<sup>42,43</sup>) was performed with the  
728 “blockwiseModules” function from the R package “WGCNA” (version 1.71) using the insulin  
729 response values of all insulin-regulated phosphopeptides. Default parameters were used except for  
730 power = 3 (determined as recommended in <sup>42</sup>), deepSplit = 3, minModuleSize = 15, reassignThreshold  
731 = 0, and mergeCutHeight = 0.25. Subnetwork eigengenes were extracted and termed “eigenpeptides”.

732 One-sided fisher’s exact tests were performed to assess the enrichment of Gene Ontology (GO)  
733 Biological Processes, GO Cellular Compartments (R package “org.Mm.eg.db” version 3.15.0<sup>82</sup>), and  
734 kinase substrates in each subnetwork relative to the entire phosphoproteome. Only pathways containing  
735 three or more subnetwork phosphoproteins were tested. Kinase substrate enrichment was performed

736 using the same annotations as KSEA. P-values were adjusted within each analysis by the Benjamini-  
737 Hochberg procedure. Subnetwork phosphopeptides were mapped into insulin signalling temporal  
738 clusters defined in our previous study of insulin signalling dynamics<sup>10</sup>, using PhosphositePlus Site  
739 Group IDs. The timepoint at which each cluster appeared to reach its maximum insulin-stimulated value  
740 was used as a measure of insulin response speed.

741

#### 742 ***Glucose uptake correlations***

743 For each insulin-regulated phosphopeptide, Pearson's correlation tests were performed to assess the  
744 linear association between <sup>3</sup>H-2DG uptake in insulin-stimulated mice and phosphopeptide insulin  
745 response values or unnormalized insulin-stimulated log2 intensity. Phosphopeptides were considered  
746 correlated with <sup>3</sup>H-2DG uptake when  $q < 0.1$  and their Pearson's correlation coefficient was of  
747 substantial magnitude ( $r > 0.35$  or  $r < -0.35$ ). Pearson's correlation tests were also performed comparing  
748 insulin-stimulated <sup>3</sup>H-2DG uptake to KSEA enrichment scores in individual mice or using the median  
749 in each strain-diet combination.

750

#### 751 ***Cell culture***

752 GLUT4-HA-L6 myoblasts<sup>83</sup> were grown in α-MEM supplemented with 10% fetal bovine serum in a  
753 humidified chamber at 37 °C, 10% CO<sub>2</sub>. Differentiation was induced by changing media to α-MEM  
754 supplemented with 2% horse serum for 5 days.

755

#### 756 ***Pfkfb3 overexpression***

757 Platinum-E (Plat-E) retroviral packaging cells were grown to confluence and transfected with 10 µg  
758 total DNA: either pBabe puromycin empty vector, pBabe puromycin Pfkfb3 or pWZL neomycin HA-  
759 GLUT4. After 48 h retroviral media was collected and passed through a 0.45 µm filter. L6 myotubes  
760 were grown to confluence and retrovirally transfected with 2 mL of HA-GLUT4 neomycin viral media  
761 in the presence of 10 µg/ml polybrene. The following morning, cells were split into growth media  
762 containing neomycin (800 µg/ml) and passaged until only successfully transfected cells remained.  
763 These cells were then grown to confluence and retrovirally transfected again with 2 mL of either empty  
764 vector puromycin viral media or Pfkfb3 puromycin viral media in the presence of 10 µg/ml of polybrene.  
765 The following morning, cells were split into growth media containing both neomycin (800 µg/ml) and  
766 puromycin (2 µg/ml) and passaged until only successfully transfected cells remained in culture.

767

#### 768 ***Extracellular acidification rate***

769 The extracellular acidification rate (ECAR) of GLUT4-HA-L6 cells myotubes was measured using  
770 Seahorse XFp miniplates and a Seahorse XF HS Mini Analyzer (Seahorse Bioscience, Copenhagen,  
771 Denmark) as previously described<sup>84</sup>. Cells incubated in palmitate or BSA control were washed twice  
772 with Krebs-Ringer Bicarbonate Buffer (Sigma, K4002) and once with standard cell culture media

773 without bicarbonate (XF-DMEM, pH 7.4). Cells were then incubated in XF-DMEM without glucose  
774 at 37°C for 1 h in a non-CO<sub>2</sub> incubator, followed by assaying in the XFp Analyzer. ECAR was  
775 measured after a 12-minute equilibration period followed by mix/wait/read cycles of 3/0/3 min. After  
776 stabilizing the baseline rates, compounds were injected to reach a final concentration of: 10 mM  
777 glucose, 5 µg/mL oligomycin, and 50 mM 2-deoxyglucose (2-DG), allowing estimation of glucose-  
778 driven glycolysis (glucose ECAR - basal ECAR), glycolytic capacity (oligomycin ECAR - 2DG  
779 ECAR), and non-glycolytic acidification (equal to 2DG ECAR). Data were normalized to protein  
780 concentration and presented as a percentage of total ECAR.

781

#### 782 ***2DG uptake in GLUT4-HA-L6 myotubes***

783 2-deoxyglucose (2DG) uptake into GLUT4-HA-L6 myotubes was performed as previously described  
784 with modifications<sup>83,85</sup>. Cells were incubated overnight in αMEM supplemented with either BSA-  
785 coupled 125 µM palmitic acid or BSA vehicle control before being washed 3x with 37 °C HEPES-  
786 buffered saline (HBS). Cells were then incubated in HBS supplemented with 10 µM unlabelled 2-  
787 deoxyglucose and either 0 or 100 nM insulin at 37°C for 15 min. Cells were then incubated for a further  
788 5 min following the addition of 0.5 µCi/ml [<sup>3</sup>H]-2-deoxyglucose in HBS. Cells were then washed on  
789 ice 5x with ice-cold PBS and lysed in 1 M NaOH. For non-specific background uptake, 1 well per  
790 condition was pre-treated with cytochalasin B. Counts were determined by Perkin Elmer Quantulus  
791 GCT Liquid Scintillation Counter (Perkin Elmer, Waltham, MA, USA). 2DG uptake was expressed  
792 relatively to protein concentration as determined by bicinchoninic acid (BCA) assay after neutralisation  
793 with 1 M HCl and subtraction of non-specific uptake.

794

#### 795 ***Immunoblotting***

796 GLUT4-HA-L6 myotubes were incubated overnight (16 h) in either BSA-conjugated 125 µM palmitate  
797 or BSA vehicle control. Cells were optionally treated with insulin as described above, and then washed  
798 in ice-cold PBS and lysed by scraping directly into 55 °C Laemmli sample buffer with 10 % (tris 2-  
799 carboxyethyl phosphine; TCEP). Samples were sonicated for 24 s (3s on/3s off) and heated at 65 °C for  
800 5 minutes. Samples were then resolved by SDS-PAGE as previously described<sup>18</sup>, transferred onto PVDF  
801 membranes and blocked in TBS-T (0.1% Tween in Tris-buffered saline) containing 5% skim milk for  
802 1 h. Membranes were then washed 3 x 10 min in TBS-T and incubated overnight in primary antibodies  
803 against Pfkfb3 (Proteintech Group; 13763-1-AP) and α-tubulin (Cell Signalling Technologies #2125;  
804 diluted 1:1000). Insulin-stimulated cells were additionally incubated in primary antibodies against  
805 pT308 Akt (Cell Signaling Technologies #2965; diluted 1:1000), pS473 Akt (Cell Signaling  
806 Technologies #9271; diluted 1:1000), total pan-Akt (Cell Signaling Technologies #9272; diluted  
807 1:1000), pS21/S9 GSK3α/β (Cell Signaling Technologies #9327; diluted 1:1000), pT246 PRAS40 (Cell  
808 Signaling Technologies #13175; diluted 1:1000), total PRAS40 (Cell Signaling Technologies #2691,  
809 diluted 1:1000, and 14-3-3 (Santa Cruz #sc-1657, diluted 1:5000). The following day membranes were

810 washed 3 x 10 min in TBS-T and incubated for 1 h in species-appropriate fluorescent antibodies.  
811 Imaging and densitometry were performed using LI-COR Image Studio.

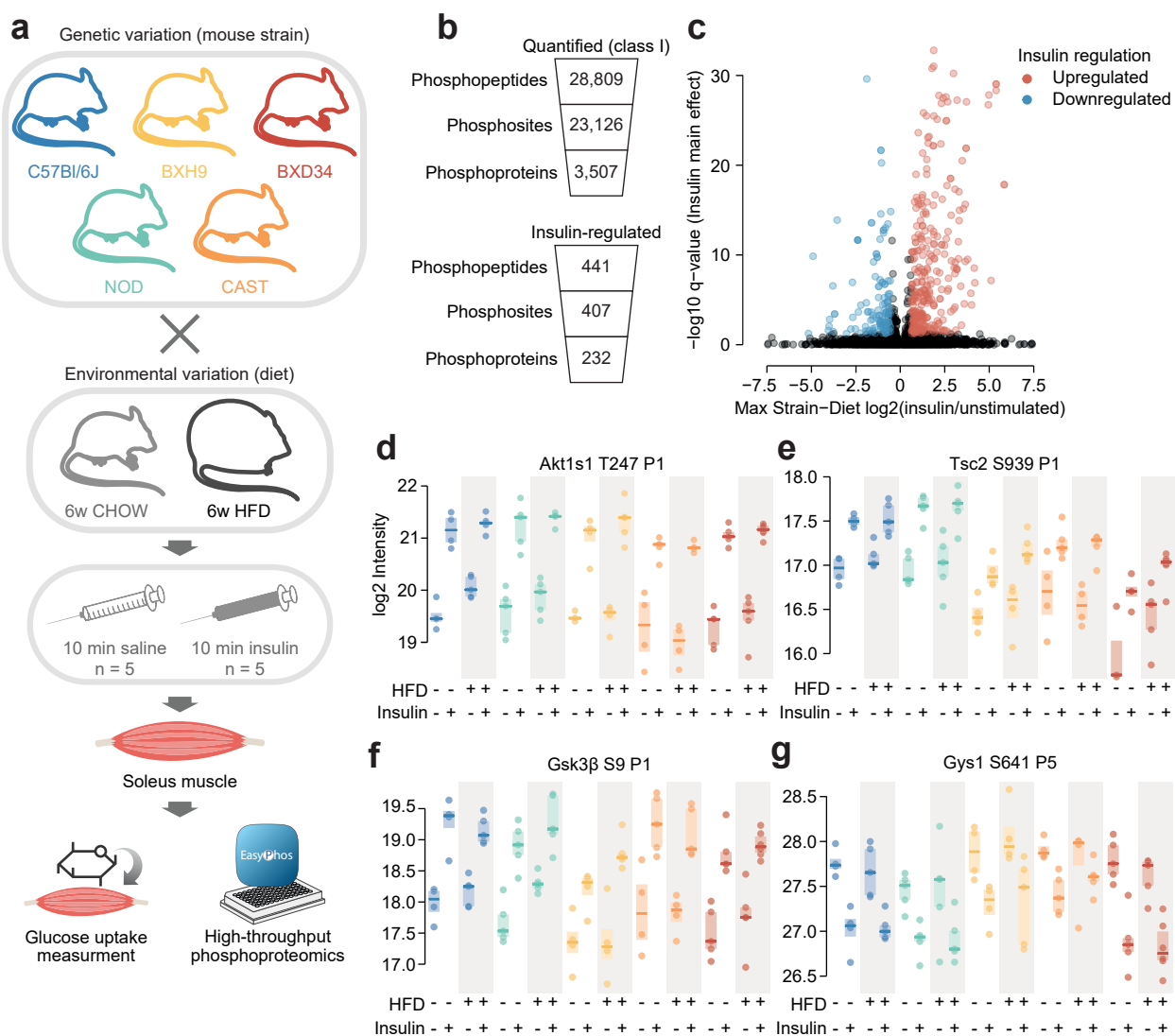


**Figure 1: Phosphoproteomics of insulin signalling in mouse skeletal muscle. a)** Workflow for skeletal muscle phosphoproteomics of insulin signalling. **b)** Quantification of skeletal muscle phosphoproteomics. **c)** Volcano plot identifying insulin-regulated phosphopeptides. The greatest  $\log_2(\text{insulin/unstimulated})$  fold change across strain-diet combinations is plotted against significance (insulin stimulation main effect, three-way ANOVA). Three phosphopeptides with  $-\log_{10} q$ -values greater than 35 were removed for visual clarity. **d-g)** Example insulin-regulated phosphopeptides. The protein and phosphorylated amino acid are indicated, as well as the number of phosphosites on the phosphopeptide (e.g. “P1”).  $n = 4-6$  biological replicates.

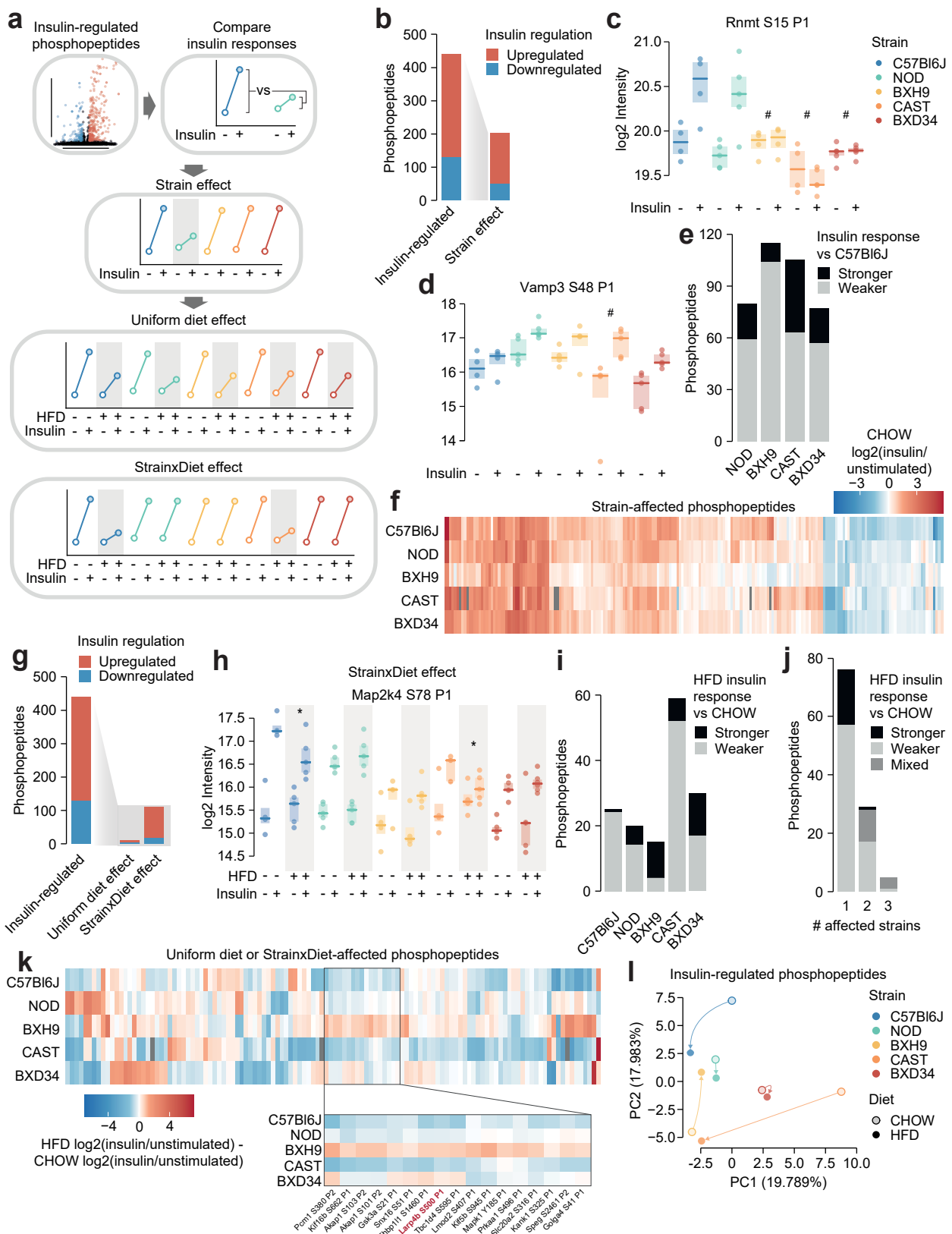


**Figure 2: Genetics and diet modulate insulin signalling.** **a)** Schematic for identifying effects of strain and diet on insulin signalling. **b)** The number of total insulin-regulated phosphopeptides and those with a Strain effect. **c-d)** Two phosphopeptides with Strain effects. ANOVAs were performed on CHOW insulin responses following two-sided t-tests comparing each strain to C57Bl6J (q-values: #). Only CHOW values are shown. **e)** The number of phosphopeptides with stronger or weaker insulin regulation in each strain compared to C57Bl6J. **f)** Heatmap displaying all insulin-regulated phosphopeptides with a Strain effect. Missing values are coloured

grey. **g)** The number of total insulin-regulated phosphopeptides and those with diet effects. **h)** A phosphopeptide with a StrainxDiet effect. A two-way ANOVA was performed on insulin response values followed by two-sided t-tests comparing HFD to CHOW within each strain (q-values: \*). **i-j)** The number of phosphopeptides with a StrainxDiet effect in **i)** each strain, or **j)** each number of strains. Colour indicates whether the insulin response in HFD is stronger vs CHOW, weaker vs CHOW, or both in different strains (“Mixed”). **k)** Heatmap displaying all insulin-regulated phosphopeptides with a Uniform diet effect or StrainxDiet effect. Inset displays example sites where BXH9 effects contrasted other strains. **l)** PCA of all insulin-regulated phosphopeptides using the  $\log_2(\text{insulin}/\text{unstimulated})$  fold changes for each Strain-Diet combination. The percentage of total variance explained by each principal component is indicated. \*/#:  $0.01 \leq q < 0.05$ , \*\*/##:  $0.001 \leq q < 0.01$ , \*\*\*/###:  $q < 0.001$ . n = 4-6 biological replicates.

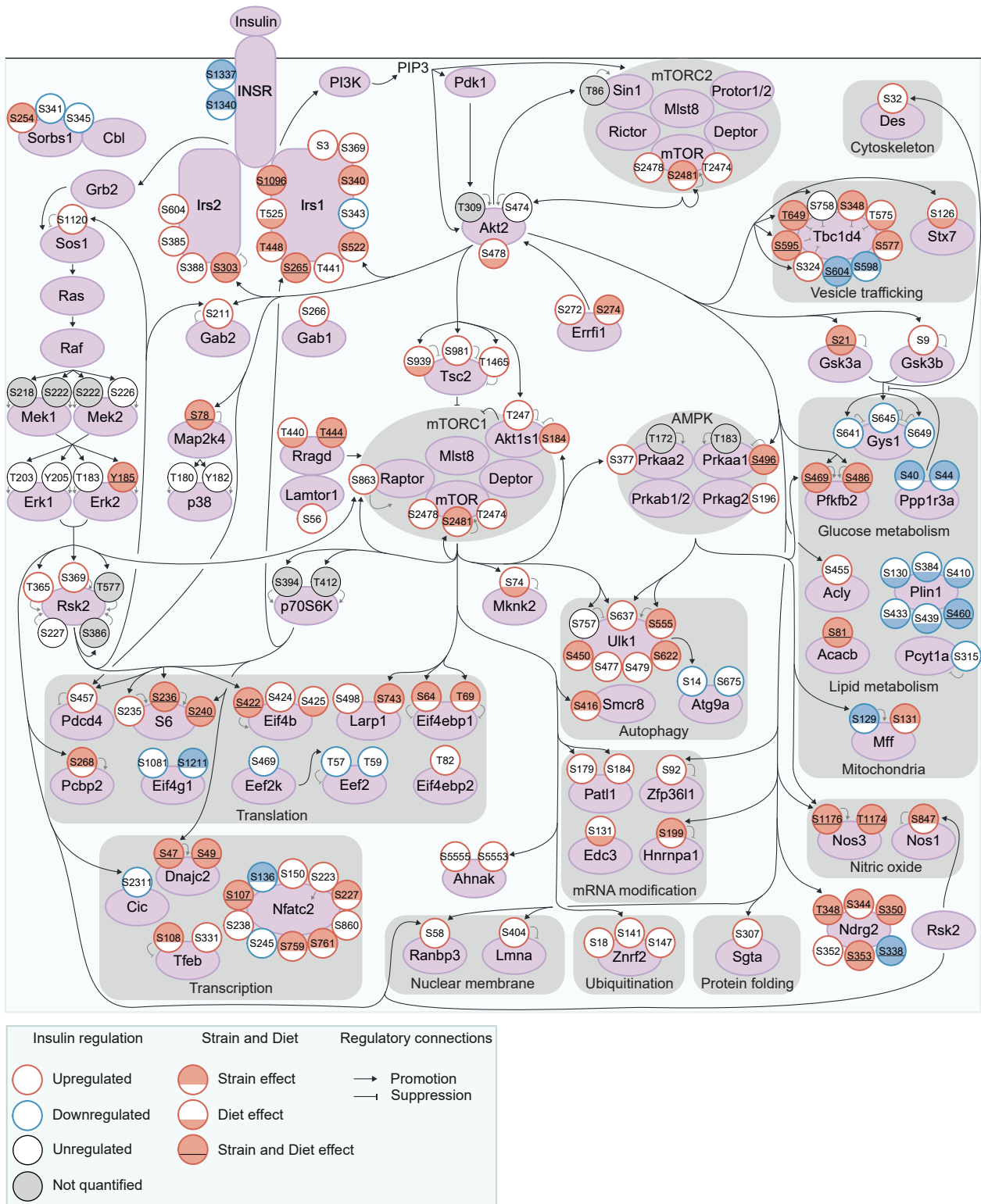


**Figure 3: Exploring genetic and dietary modulation of the insulin signalling network.** A curated network of 160 insulin-regulated phosphosites. Phosphosites are depicted as circles where the outline colour denotes the direction of insulin regulation, and the inner colour denotes the presence of Strain effects or Diet effects (either a StrainxDiet or Uniform diet effect). Black arrows indicate regulatory relationships from proteins to other proteins or phosphosites. Grey lines indicate phosphosite regulatory roles.

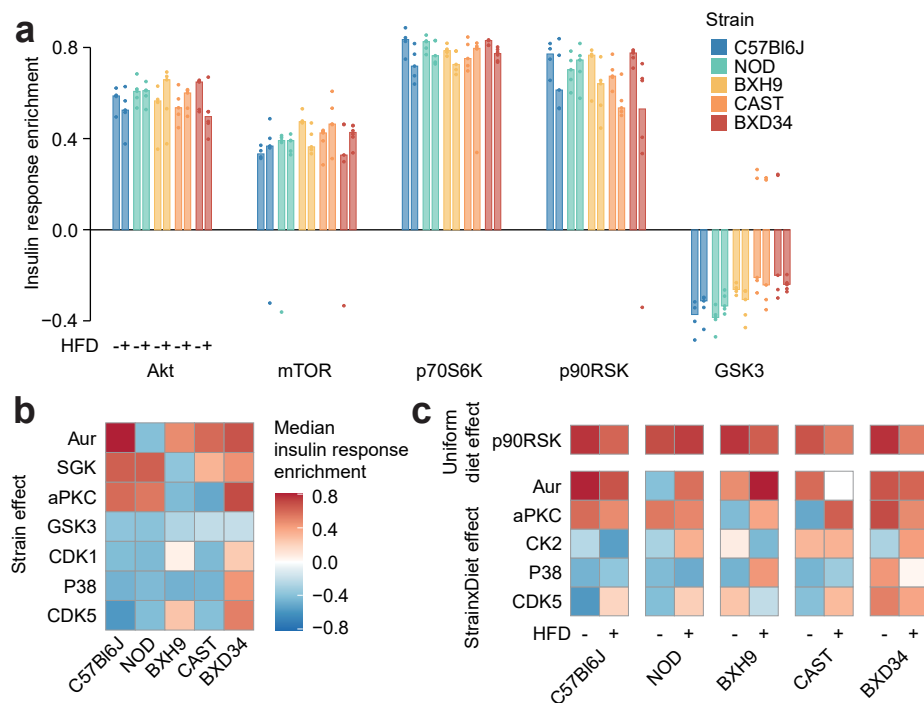


**Figure 4: Genetics and diet rewire insulin-regulated kinase signalling.** **a)** Kinase substrate enrichment analysis (KSEA)<sup>37</sup> of five canonical insulin-regulated kinases using insulin response values and kinase-substrate annotations from PhosphositePlus<sup>32</sup>. **b-c)** Kinase enrichment scores were tested for **b)** Strain effects (CHOW ANOVA adjusted  $p < 0.05$ ) or **c)** StrainxDiet effects (two-way ANOVA interaction effect adjusted  $p < 0.05$ ) and Uniform diet effects (Diet main effect adjusted  $p < 0.05$ , interaction effect adjusted  $p \geq 0.05$ ).  $n = 4-6$  biological replicates.

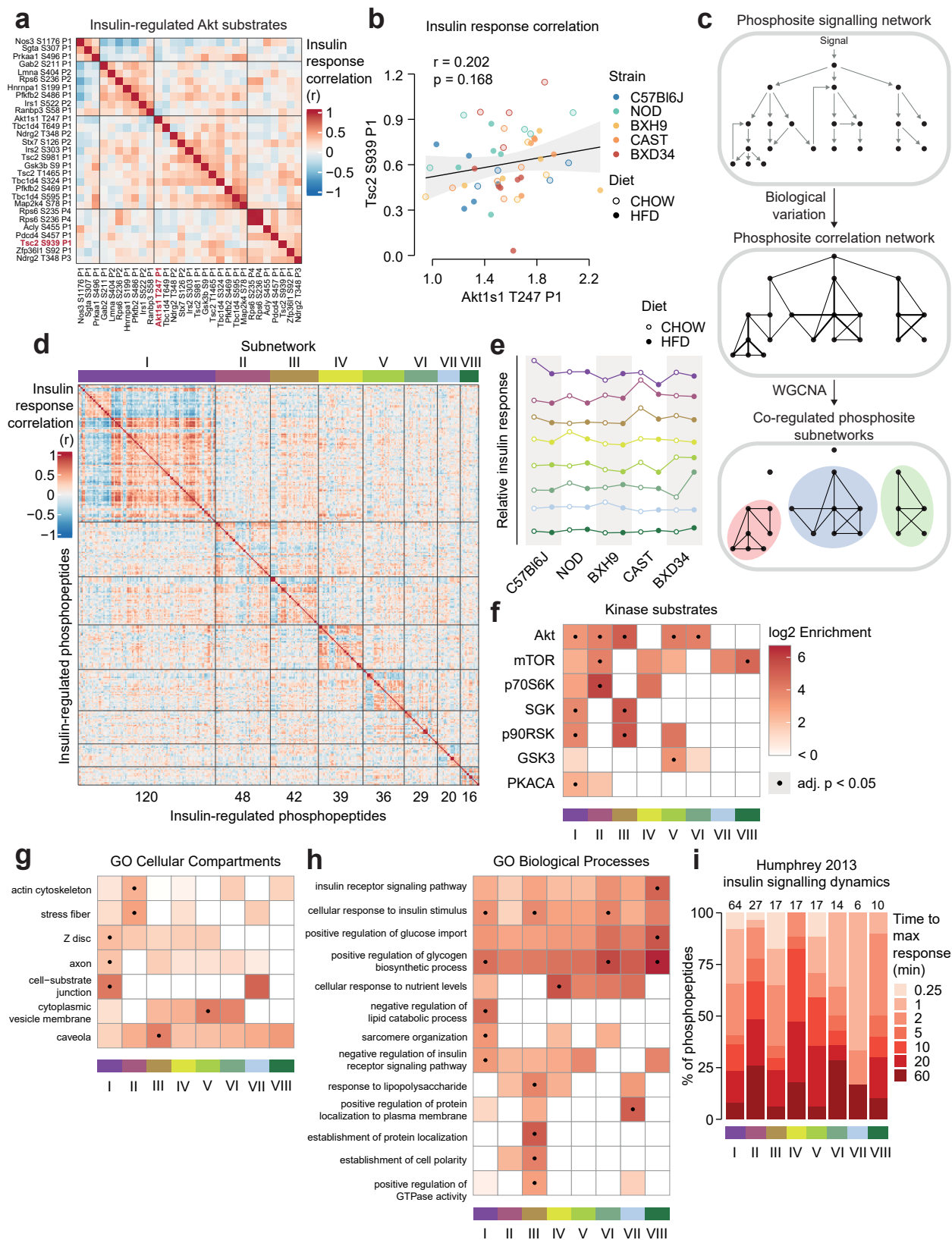


**Figure 5: Biological variation reveals functional organisation of the insulin signalling network.**

**a)** Pairwise Pearson's correlation of the insulin response values of insulin-regulated Akt substrates. Substrates were separated into four clusters by hierarchical clustering followed by tree cutting. **b)** The correlation between insulin response values of the Akt substrates Tsc2 S939 and Akt1s1 T247. Linear regression is indicated with 95% confidence intervals. **c)** Rationale for performing WGCNA. **d)** Pairwise Pearson's correlation of all insulin-regulated phosphopeptides separated into WGCNA-derived subnetworks. The number of

phosphopeptides in each subnetwork is indicated below the heatmap. **e)** The “eigenpeptide” of each subnetwork. The median of each strain-diet combination is shown. **f-h)** The enrichment of **f)** PhosphositePlus-derived kinase-substrate annotations<sup>32</sup>, **g)** GO cellular compartments, and **h)** GO biological processes within each subnetwork relative to the entire phosphoproteome (one-sided Fisher’s exact test, Benjamini-Hochberg p-value adjustment). **i)** The time taken for phosphopeptides to reach maximum insulin-stimulated intensity in a previous study of insulin signalling dynamics<sup>10</sup>. The number of phosphopeptides mapped into the study is indicated above each bar.

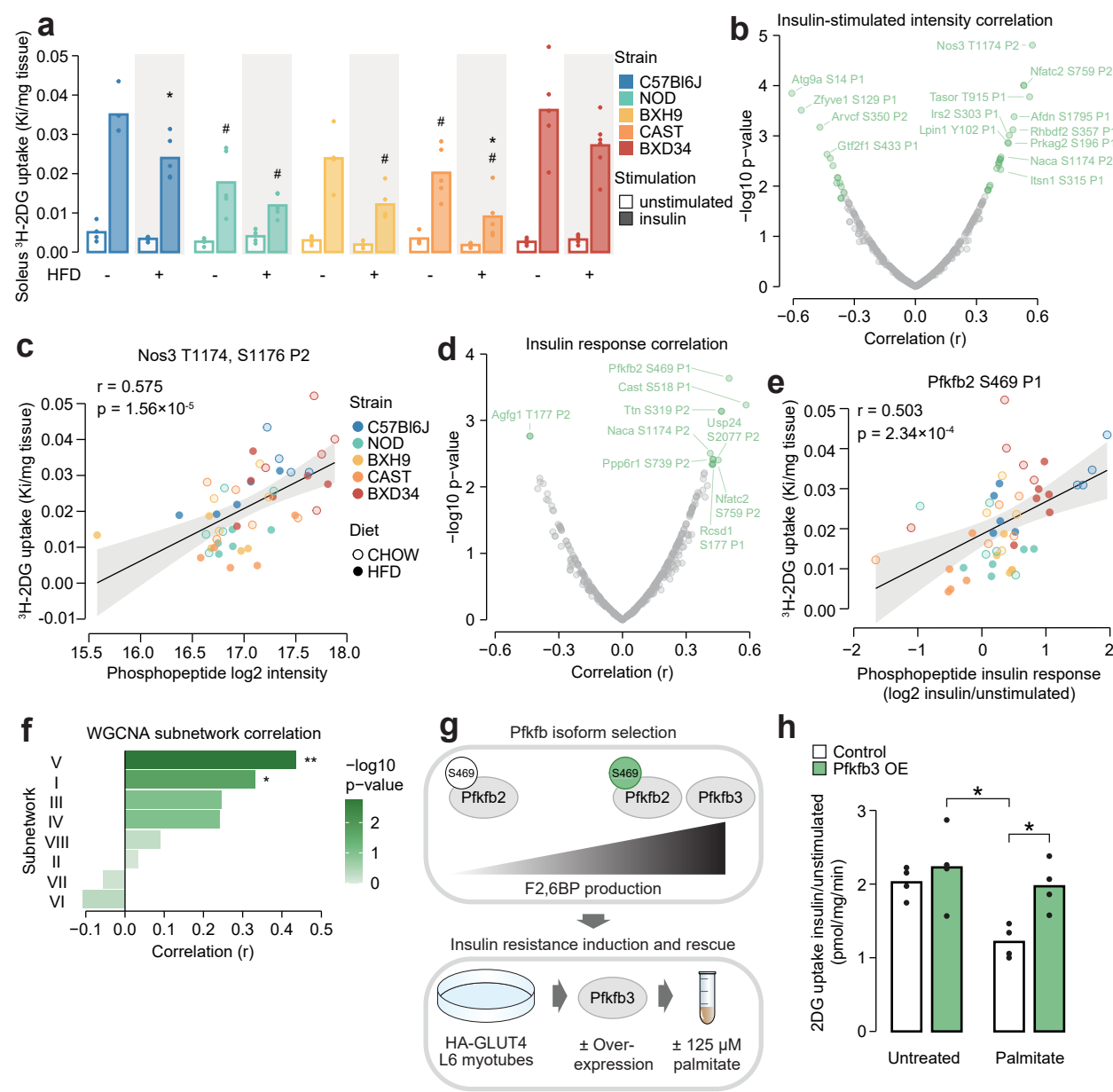


**Figure 6: Leveraging biological variation to identify drivers of insulin responsiveness.** **a)** The uptake of  $^3\text{H}$ -2DG into mouse soleus muscle after a 10 min injection of insulin (1 U/kg lean mass; “insulin”) or saline (“unstimulated”) calculated as a rate constant (Ki). Two-sided t-tests were performed on insulin-stimulated uptake values to compare HFD to CHOW within each strain (adjusted p-value: \*) or each strain to C57Bl6J within either diet (adjusted p-value: #). n = 4-6 biological replicates. **b)** Pearson’s correlation between log<sub>2</sub> intensity of insulin-regulated phosphopeptides and  $^3\text{H}$ -2DG uptake within insulin-stimulated mice. Significantly correlated phosphopeptides (q-value < 0.1, r > 0.35 or r < -0.35) are coloured green and select correlated phosphopeptides are labelled. **c)** Correlation of Nos3 T1174, S1176 insulin-stimulated intensity with insulin-stimulated  $^3\text{H}$ -2DG uptake. Linear regression is indicated with 95% confidence intervals. **d)** As in **b**, using phosphopeptide insulin response values. **e)** Correlation of the Pfkfb2 S469 insulin response with insulin-stimulated  $^3\text{H}$ -2DG uptake. **f)** Correlation of WGCNA subnetwork eigenpeptides with insulin-stimulated  $^3\text{H}$ -2DG uptake. Significant correlations are indicated (\*). **g)** Rationale and workflow for over-expressing Pfkfb3 to rescue palmitate-induced insulin resistance. **h)** The fold change of unstimulated to insulin-stimulated glucose uptake (100 nM insulin, 20 min) in L6-GLUT4-HA myotubes with or without Pfkfb3 overexpression, treated with palmitate (125  $\mu\text{M}$ , 16 h) or BSA vehicle control. A two-way ANOVA was performed followed by

Tukey's posthoc tests (\*). Not all significant comparisons are shown. n = 4 biological replicates. \*/#:  $0.01 \leq p < 0.05$ , \*\*/##:  $0.001 \leq p < 0.01$ , \*\*\*/###:  $p < 0.001$

812

813 **References**

- 814 1. Humphrey, S.J., James, D.E., and Mann, M. (2015). Protein Phosphorylation: A Major Switch  
815 Mechanism for Metabolic Regulation. *Trends Endocrinol. Metab.* *26*, 676–687.
- 816 2. Needham, E.J., Parker, B.L., Burykin, T., James, D.E., and Humphrey, S.J. (2019). Illuminating  
817 the dark phosphoproteome. *Sci. Signal.* *12*. 10.1126/scisignal.aau8645.
- 818 3. Olsen, J.V., Blagoev, B., Gnad, F., Macek, B., Kumar, C., Mortensen, P., and Mann, M. (2006).  
819 Global, *in vivo*, and site-specific phosphorylation dynamics in signaling networks. *Cell* *127*, 635–  
820 648.
- 821 4. Bodenmiller, B., Wanka, S., Kraft, C., Urban, J., Campbell, D., Pedrioli, P.G., Gerrits, B., Picotti,  
822 P., Lam, H., Vitek, O., Brusniak, M.-Y., Roschitzki, B., Zhang, C., Shokat, K.M., Schlapbach, R.,  
823 Colman-Lerner, A., Nolan, G.P., Nesvizhskii, A.I., Peter, M., Loewith, R., von Mering, C., and  
824 Aebersold, R. (2010). Phosphoproteomic analysis reveals interconnected system-wide responses  
825 to perturbations of kinases and phosphatases in yeast. *Sci. Signal.* *3*, rs4.
- 826 5. Needham, E.J., Humphrey, S.J., Cooke, K.C., Fazakerley, D.J., Duan, X., Parker, B.L., and James,  
827 D.E. (2019). Phosphoproteomics of Acute Cell Stressors Targeting Exercise Signaling Networks  
828 Reveal Drug Interactions Regulating Protein Secretion. *Cell Rep.* *29*, 1524–1538.e6.
- 829 6. Leutert, M., Barente, A.S., Fukuda, N.K., Rodriguez-Mias, R.A., and Villén, J. (2022). The  
830 regulatory landscape of the yeast phosphoproteome. *bioRxiv*, 2022.10.23.513432.  
831 10.1101/2022.10.23.513432.
- 832 7. Haeusler, R.A., McGraw, T.E., and Accili, D. (2018). Biochemical and cellular properties of  
833 insulin receptor signalling. *Nat. Rev. Mol. Cell Biol.* *19*, 31–44.
- 834 8. Gehart, H., Kumpf, S., Ittner, A., and Ricci, R. (2010). MAPK signalling in cellular metabolism:  
835 stress or wellness? *EMBO Rep.* *11*, 834–840.
- 836 9. Sylow, L., Jensen, T.E., Kleinert, M., Højlund, K., Kiens, B., Wojtaszewski, J., Prats, C.,  
837 Schjerling, P., and Richter, E.A. (2013). Rac1 signaling is required for insulin-stimulated glucose  
838 uptake and is dysregulated in insulin-resistant murine and human skeletal muscle. *Diabetes* *62*,  
839 1865–1875.
- 840 10. Humphrey, S.J., Yang, G., Yang, P., Fazakerley, D.J., Stöckli, J., Yang, J.Y., and James, D.E.  
841 (2013). Dynamic adipocyte phosphoproteome reveals that Akt directly regulates mTORC2. *Cell  
842 Metab.* *17*, 1009–1020.
- 843 11. Humphrey, S.J., Azimifar, S.B., and Mann, M. (2015). High-throughput phosphoproteomics  
844 reveals *in vivo* insulin signaling dynamics. *Nat. Biotechnol.* *33*, 990–995.
- 845 12. Krüger, M., Kratchmarova, I., Blagoev, B., Tseng, Y.-H., Kahn, C.R., and Mann, M. (2008).  
846 Dissection of the insulin signaling pathway via quantitative phosphoproteomics. *Proc. Natl. Acad.  
847 Sci. U. S. A.* *105*, 2451–2456.
- 848 13. James, D.E., Stöckli, J., and Birnbaum, M.J. (2021). The aetiology and molecular landscape of  
849 insulin resistance. *Nat. Rev. Mol. Cell Biol.* 10.1038/s41580-021-00390-6.
- 850 14. Fazakerley, D.J., Krycer, J.R., Kearney, A.L., Hocking, S.L., and James, D.E. (2019). Muscle and  
851 adipose tissue insulin resistance: malady without mechanism? *J. Lipid Res.* *60*, 1720–1732.
- 852 15. van Gerwen, J., Shun-Shion, A.S., and Fazakerley, D.J. (2023). Insulin signalling and GLUT4  
853 trafficking in insulin resistance. *Biochem. Soc. Trans.* *51*, 1057–1069.

854 16. Hunter, D.J. (2005). Gene–environment interactions in human diseases. *Nat. Rev. Genet.* *6*, 287–  
855 298.

856 17. Civelek, M., and Lusis, A.J. (2014). Systems genetics approaches to understand complex traits. *Nat. Rev. Genet.* *15*, 34–48.

858 18. Nelson, M.E., Madsen, S., Cooke, K.C., Fritzen, A.M., Thorius, I.H., Masson, S.W.C., Carroll, L.,  
859 Weiss, F.C., Seldin, M.M., Potter, M., Hocking, S.L., Fazakerley, D.J., Brandon, A.E.,  
860 Thillainadesan, S., Senior, A.M., Cooney, G.J., Stöckli, J., and James, D.E. (2022). Systems-level  
861 analysis of insulin action in mouse strains provides insight into tissue- and pathway-specific  
862 interactions that drive insulin resistance. *Cell Metab.* *34*, 227–239.e6.

863 19. Montgomery, M.K., Hallahan, N.L., Brown, S.H., Liu, M., Mitchell, T.W., Cooney, G.J., and  
864 Turner, N. (2013). Mouse strain-dependent variation in obesity and glucose homeostasis in  
865 response to high-fat feeding. *Diabetologia* *56*, 1129–1139.

866 20. Grossbach, J., Gillet, L., Clément-Ziza, M., Schmalohr, C.L., Schubert, O.T., Schütter, M., Mawer,  
867 J.S.P., Barnes, C.A., Bludau, I., Weith, M., Tessarz, P., Graef, M., Aebersold, R., and Beyer, A.  
868 (2022). The impact of genomic variation on protein phosphorylation states and regulatory  
869 networks. *Mol. Syst. Biol.* *18*, e10712.

870 21. Zhang, T., Keele, G.R., Gyuricza, I.G., Vincent, M., Brunton, C., Bell, T.A., Hock, P., Shaw, G.D.,  
871 Munger, S.C., de Villena, F.P.-M., Ferris, M.T., Paulo, J.A., Gygi, S.P., and Churchill, G.A. (2023).  
872 Multi-omics analysis identifies drivers of protein phosphorylation. *Genome Biol.* *24*, 52.

873 22. Needham, E.J., Hingst, J.R., Parker, B.L., Morrison, K.R., Yang, G., Onslev, J., Kristensen, J.M.,  
874 Højlund, K., Ling, N.X.Y., Oakhill, J.S., Richter, E.A., Kiens, B., Petersen, J., Pehmøller, C.,  
875 James, D.E., Wojtaszewski, J.F.P., and Humphrey, S.J. (2021). Personalized phosphoproteomics  
876 identifies functional signaling. *Nat. Biotechnol.* *10*.1038/s41587-021-01099-9.

877 23. McCarthy, M.I., Abecasis, G.R., Cardon, L.R., Goldstein, D.B., Little, J., Ioannidis, J.P.A., and  
878 Hirschhorn, J.N. (2008). Genome-wide association studies for complex traits: consensus,  
879 uncertainty and challenges. *Nat. Rev. Genet.* *9*, 356–369.

880 24. Lusis, A.J., Seldin, M.M., Allayee, H., Bennett, B.J., Civelek, M., Davis, R.C., Eskin, E., Farber,  
881 C.R., Hui, S., Mehrabian, M., Norheim, F., Pan, C., Parks, B., Rau, C.D., Smith, D.J., Vallim, T.,  
882 Wang, Y., and Wang, J. (2016). The Hybrid Mouse Diversity Panel: a resource for systems  
883 genetics analyses of metabolic and cardiovascular traits. *J. Lipid Res.* *57*, 925–942.

884 25. Burchfield, J.G., Kebede, M.A., Meoli, C.C., Stöckli, J., Tess Whitworth, P., Wright, A.L.,  
885 Hoffman, N.J., Minard, A.Y., Ma, X., Krycer, J.R., Nelson, M.E., Tan, S.-X., Yau, B., Thomas,  
886 K.C., Wee, N.K.Y., Khor, E.-C., Enriquez, R.F., Vissel, B., Biden, T.J., Baldock, P.A., Hoehn,  
887 K.L., Cantley, J., Cooney, G.J., James, D.E., and Fazakerley, D.J. (2018). High dietary fat and  
888 sucrose result in an extensive and time-dependent deterioration in health of multiple physiological  
889 systems in mice. *J. Biol. Chem.* *293*, 5731–5745.

890 26. DeFronzo, R.A. (1988). The Triumvirate: β-Cell, Muscle, Liver: A Collusion Responsible for  
891 NIDDM. *Diabetes* *37*, 667–687.

892 27. Schiaffino, S., and Reggiani, C. (2011). Fiber types in mammalian skeletal muscles. *Physiol. Rev.*  
893 *91*, 1447–1531.

894 28. Humphrey, S.J., Karayel, O., James, D.E., and Mann, M. (2018). High-throughput and high-  
895 sensitivity phosphoproteomics with the EasyPhos platform. *Nat. Protoc.* *13*, 1897–1916.

896 29. Bekker-Jensen, D.B., Bernhardt, O.M., Hogrebe, A., Martinez-Val, A., Verbeke, L., Gandhi, T.,  
897 Kelstrup, C.D., Reiter, L., and Olsen, J.V. (2020). Rapid and site-specific deep phosphoproteome

898 profiling by data-independent acquisition without the need for spectral libraries. *Nat. Commun.* *11*,  
899 787.

900 30. Batista, T.M., Jayavelu, A.K., Wewer Albrechtsen, N.J., Iovino, S., Lebastchi, J., Pan, H., Dreyfuss,  
901 J.M., Krook, A., Zierath, J.R., Mann, M., and Kahn, C.R. (2020). A Cell-Autonomous Signature  
902 of Dysregulated Protein Phosphorylation Underlies Muscle Insulin Resistance in Type 2 Diabetes.  
903 *Cell Metab.* *32*, 844–859.e5.

904 31. Haider, N., Lebastchi, J., Jayavelu, A.K., Batista, T.M., Pan, H., Dreyfuss, J.M., Carcamo-Orive,  
905 I., Knowles, J.W., Mann, M., and Kahn, C.R. (2021). Signaling defects associated with insulin  
906 resistance in non-diabetic and diabetic individuals and modification by sex. *J. Clin. Invest.*  
907 10.1172/JCI151818.

908 32. Fazakerley, D.J., van Gerwen, J., Cooke, K.C., Duan, X., Needham, E.J., Díaz-Vegas, A., Madsen,  
909 S., Norris, D.M., Shun-Shion, A.S., Krycer, J.R., Burchfield, J.G., Yang, P., Wade, M.R.,  
910 Brozinick, J.T., James, D.E., and Humphrey, S.J. (2023). Phosphoproteomics reveals rewiring of  
911 the insulin signaling network and multi-nodal defects in insulin resistance. *Nat. Commun.* *14*, 1–  
912 20.

913 33. Hornbeck, P.V., Zhang, B., Murray, B., Kornhauser, J.M., Latham, V., and Skrzypek, E. (2015).  
914 PhosphoSitePlus, 2014: mutations, PTMs and recalibrations. *Nucleic Acids Res.* *43*, D512–20.

915 34. Klip, A., McGraw, T.E., and James, D.E. (2019). Thirty sweet years of GLUT4. *J. Biol. Chem.*  
916 294, 11369–11381.

917 35. Hoffman, N.J., Parker, B.L., Chaudhuri, R., Fisher-Wellman, K.H., Kleinert, M., Humphrey, S.J.,  
918 Yang, P., Holliday, M., Trefely, S., Fazakerley, D.J., Stöckli, J., Burchfield, J.G., Jensen, T.E.,  
919 Jothi, R., Kiens, B., Wojtaszewski, J.F.P., Richter, E.A., and James, D.E. (2015). Global  
920 Phosphoproteomic Analysis of Human Skeletal Muscle Reveals a Network of Exercise-Regulated  
921 Kinases and AMPK Substrates. *Cell Metab.* *22*, 922–935.

922 36. Ochoa, D., Jarnuczak, A.F., Viéitez, C., Gehre, M., Soucheray, M., Mateus, A., Kleefeldt, A.A.,  
923 Hill, A., Garcia-Alonso, L., Stein, F., Krogan, N.J., Savitski, M.M., Swaney, D.L., Vizcaíno, J.A.,  
924 Noh, K.-M., and Beltrao, P. (2020). The functional landscape of the human phosphoproteome. *Nat.*  
925 *Biotechnol.* *38*, 365–373.

926 37. Schwenk, R.W., Angin, Y., Steinbusch, L.K.M., Dirkx, E., Hoebers, N., Coumans, W.A., Bonen,  
927 A., Broers, J.L.V., van Eys, G.J., Glatz, J.F.C., and Others (2012). Overexpression of vesicle-  
928 associated membrane protein (VAMP) 3, but not VAMP2, protects glucose transporter (GLUT) 4  
929 protein translocation in an in vitro model of cardiac insulin resistance. *J. Biol. Chem.* *287*, 37530–  
930 37539.

931 38. Barilari, M., Bonfils, G., Treins, C., Koka, V., De Villeneuve, D., Fabrega, S., and Pende, M.  
932 (2017). ZRF1 is a novel S6 kinase substrate that drives the senescence programme. *EMBO J.* *36*,  
933 736–750.

934 39. Agassandian, M., Zhou, J., Tephly, L.A., Ryan, A.J., Carter, A.B., and Mallampalli, R.K. (2005).  
935 Oxysterols inhibit phosphatidylcholine synthesis via ERK docking and phosphorylation of  
936 CTP:phosphocholine cytidylyltransferase. *J. Biol. Chem.* *280*, 21577–21587.

937 40. Hernandez-Armenta, C., Ochoa, D., Gonçalves, E., Saez-Rodriguez, J., and Beltrao, P. (2017).  
938 Benchmarking substrate-based kinase activity inference using phosphoproteomic data.  
939 *Bioinformatics* *33*, 1845–1851.

940 41. Tonks, K.T., Ng, Y., Miller, S., Coster, A.C.F., Samocha-Bonet, D., Iseli, T.J., Xu, A., Patrick, E.,  
941 Yang, J.Y.H., Junutula, J.R., Modrusan, Z., Kolumam, G., Stöckli, J., Chisholm, D.J., James, D.E.,

942 and Greenfield, J.R. (2013). Impaired Akt phosphorylation in insulin-resistant human muscle is  
943 accompanied by selective and heterogeneous downstream defects. *Diabetologia* 56, 875–885.

944 42. Zhang, B., and Horvath, S. (2005). A General Framework for Weighted Gene Co-Expression  
945 Network Analysis. *Statistical Applications in Genetics and Molecular Biology* 4. 10.2202/1544-  
946 6115.1128.

947 43. Langfelder, P., and Horvath, S. (2008). WGCNA: an R package for weighted correlation network  
948 analysis. *BMC Bioinformatics* 9, 559.

949 44. Roy, D., Perreault, M., and Marette, A. (1998). Insulin stimulation of glucose uptake in skeletal  
950 muscles and adipose tissues in vivo is NO dependent. *Am. J. Physiol.* 274, E692-9.

951 45. Bahadoran, Z., Mirmiran, P., and Ghasemi, A. (2020). Role of Nitric Oxide in Insulin Secretion  
952 and Glucose Metabolism. *Trends Endocrinol. Metab.* 31, 118–130.

953 46. Dimmeler, S., Fleming, I., Fisslthaler, B., Hermann, C., Busse, R., and Zeiher, A.M. (1999).  
954 Activation of nitric oxide synthase in endothelial cells by Akt-dependent phosphorylation. *Nature*  
955 399, 601–605.

956 47. Lundh, M., Petersen, P.S., Isidor, M.S., Kazoka-Sørensen, D.N., Plucińska, K., Shamsi, F., Ørskov,  
957 C., Tozzi, M., Brown, E.L., Andersen, E., Ma, T., Müller, U., Barrès, R., Kristiansen, V.B.,  
958 Gerhart-Hines, Z., Tseng, Y.-H., and Emanuelli, B. (2019). Afadin is a scaffold protein repressing  
959 insulin action via HDAC6 in adipose tissue. *EMBO Rep.* 20, e48216.

960 48. O'Neill, H.M. (2013). AMPK and Exercise: Glucose Uptake and Insulin Sensitivity. *Diabetes*  
961 *Metab. J.* 37, 1–21.

962 49. Deprez, J., Vertommen, D., Alessi, D.R., Hue, L., and Rider, M.H. (1997). Phosphorylation and  
963 activation of heart 6-phosphofructo-2-kinase by protein kinase B and other protein kinases of the  
964 insulin signaling cascades. *J. Biol. Chem.* 272, 17269–17275.

965 50. Marsin, A.-S., Bertrand, L., Rider, M.H., Deprez, J., Beauloye, C., Vincent, M.F., Van den Berghe,  
966 G., Carling, D., and Hue, L. (2000). Phosphorylation and activation of heart PFK-2 by AMPK has  
967 a role in the stimulation of glycolysis during ischaemia. *Curr. Biol.* 10, 1247–1255.

968 51. Ros, S., and Schulze, A. (2013). Balancing glycolytic flux: the role of 6-phosphofructo-2-  
969 kinase/fructose 2,6-bisphosphatases in cancer metabolism. *Cancer Metab* 1, 8.

970 52. Stöckli, J., Fazakerley, D.J., and James, D.E. (2011). GLUT4 exocytosis. *J. Cell Sci.* 124, 4147–  
971 4159.

972 53. Dokken, B.B., Sloniger, J.A., and Henriksen, E.J. (2005). Acute selective glycogen synthase  
973 kinase-3 inhibition enhances insulin signaling in prediabetic insulin-resistant rat skeletal muscle.  
974 *Am. J. Physiol. Endocrinol. Metab.* 288, E1188-94.

975 54. Henriksen, E.J., and Teachey, M.K. (2007). Short-term in vitro inhibition of glycogen synthase  
976 kinase 3 potentiates insulin signaling in type I skeletal muscle of Zucker Diabetic Fatty rats.  
977 *Metabolism* 56, 931–938.

978 55. Ring, D.B., Johnson, K.W., Henriksen, E.J., Nuss, J.M., Goff, D., Kinnick, T.R., Ma, S.T., Reeder,  
979 J.W., Samuels, I., Slabiak, T., Wagman, A.S., Hammond, M.-E.W., and Harrison, S.D. (2003).  
980 Selective glycogen synthase kinase 3 inhibitors potentiate insulin activation of glucose transport  
981 and utilization in vitro and in vivo. *Diabetes* 52, 588–595.

982 56. Masson, S.W.C., Madsen, S., Cooke, K.C., Potter, M., Vegas, A.D., Carroll, L., Thillainadesan,  
983 S., Cutler, H.B., Walder, K.R., Cooney, G.J., Morahan, G., Stöckli, J., and James, D.E. (2023).

984 985 Leveraging genetic diversity to identify small molecules that reverse mouse skeletal muscle insulin  
resistance. *Elife* 12. 10.7554/eLife.86961.

986 987 988 989 990 57. Trefely, S., Khoo, P.-S., Krycer, J.R., Chaudhuri, R., Fazakerley, D.J., Parker, B.L., Sultani, G., Lee, J., Stephan, J.-P., Torres, E., Jung, K., Kuijl, C., James, D.E., Junutula, J.R., and Stöckli, J. (2015). Kinome Screen Identifies PFKFB3 and Glucose Metabolism as Important Regulators of the Insulin/Insulin-like Growth Factor (IGF)-1 Signaling Pathway. *J. Biol. Chem.* 290, 25834–25846.

991 992 58. Dephoure, N., Gould, K.L., Gygi, S.P., and Kellogg, D.R. (2013). Mapping and analysis of phosphorylation sites: a quick guide for cell biologists. *Mol. Biol. Cell* 24, 535–542.

993 994 995 996 59. Hoehn, K.L., Salmon, A.B., Hohnen-Behrens, C., Turner, N., Hoy, A.J., Maghzal, G.J., Stocker, R., Van Remmen, H., Kraegen, E.W., Cooney, G.J., Richardson, A.R., and James, D.E. (2009). Insulin resistance is a cellular antioxidant defense mechanism. *Proc. Natl. Acad. Sci. U. S. A.* 106, 17787–17792.

997 998 999 60. Tortorella, L.L., and Pilch, P.F. (2002). C2C12 myocytes lack an insulin-responsive vesicular compartment despite dexamethasone-induced GLUT4 expression. *Am. J. Physiol. Endocrinol. Metab.* 283, E514-24.

1000 1001 1002 61. Portiér, G.L., Benders, A.G., Oosterhof, A., Veerkamp, J.H., and van Kuppevelt, T.H. (1999). Differentiation markers of mouse C2C12 and rat L6 myogenic cell lines and the effect of the differentiation medium. *In Vitro Cell. Dev. Biol. Anim.* 35, 219–227.

1003 1004 62. Bloom, J., and Cross, F.R. (2007). Multiple levels of cyclin specificity in cell-cycle control. *Nat. Rev. Mol. Cell Biol.* 8, 149–160.

1005 1006 63. Steinberg, G.R., and Hardie, D.G. (2023). New insights into activation and function of the AMPK. *Nat. Rev. Mol. Cell Biol.* 24, 255–272.

1007 1008 64. Lavoie, H., Gagnon, J., and Therrien, M. (2020). ERK signalling: a master regulator of cell behaviour, life and fate. *Nat. Rev. Mol. Cell Biol.* 21, 607–632.

1009 1010 65. Meyuhas, O. (2015). Ribosomal Protein S6 Phosphorylation: Four Decades of Research. *Int. Rev. Cell Mol. Biol.* 320, 41–73.

1011 1012 1013 1014 1015 1016 1017 1018 66. Johnson, J.L., Yaron, T.M., Huntsman, E.M., Kerelsky, A., Song, J., Regev, A., Lin, T.-Y., Liberatore, K., Cizin, D.M., Cohen, B.M., Vasan, N., Ma, Y., Krismer, K., Robles, J.T., van de Kooij, B., van Vlimmeren, A.E., Andrée-Busch, N., Käufer, N.F., Dorovkov, M.V., Ryazanov, A.G., Takagi, Y., Kastenhuber, E.R., Goncalves, M.D., Hopkins, B.D., Elemento, O., Taatjes, D.J., Maucuer, A., Yamashita, A., Degterev, A., Uduman, M., Lu, J., Landry, S.D., Zhang, B., Cossentino, I., Linding, R., Blenis, J., Hornbeck, P.V., Turk, B.E., Yaffe, M.B., and Cantley, L.C. (2023). An atlas of substrate specificities for the human serine/threonine kinase. *Nature* 613, 759–766.

1019 1020 1021 1022 1023 1024 1025 1026 1027 1028 1029 67. Chen, J., Spracklen, C.N., Marenne, G., Varshney, A., Corbin, L.J., Luan, J., Willems, S.M., Wu, Y., Zhang, X., Horikoshi, M., Boutin, T.S., Mägi, R., Waage, J., Li-Gao, R., Chan, K.H.K., Yao, J., Anasanti, M.D., Chu, A.Y., Claringbould, A., Heikkinen, J., Hong, J., Hottenga, J.-J., Huo, S., Kaakinen, M.A., Louie, T., März, W., Moreno-Macias, H., Ndungu, A., Nelson, S.C., Nolte, I.M., North, K.E., Raulerson, C.K., Ray, D., Rohde, R., Rybin, D., Schurmann, C., Sim, X., Southam, L., Stewart, I.D., Wang, C.A., Wang, Y., Wu, P., Zhang, W., Ahluwalia, T.S., Appel, E.V.R., Bielak, L.F., Brody, J.A., Burtt, N.P., Cabrera, C.P., Cade, B.E., Chai, J.F., Chai, X., Chang, L.-C., Chen, C.-H., Chen, B.H., Chitrala, K.N., Chiu, Y.-F., de Haan, H.G., Delgado, G.E., Demirkhan, A., Duan, Q., Engmann, J., Fatumo, S.A., Gayán, J., Giulianini, F., Gong, J.H., Gustafsson, S., Hai, Y., Hartwig, F.P., He, J., Heianza, Y., Huang, T., Huerta-Chagoya, A., Hwang, M.Y., Jensen, R.A., Kawaguchi, T., Kentistou, K.A., Kim, Y.J., Kleber, M.E., Kooner, I.K., Lai, S., Lange, L.A.,

1030 Langefeld, C.D., Lauzon, M., Li, M., Lighart, S., Liu, J., Loh, M., Long, J., Lyssenko, V.,  
1031 Mangino, M., Marzi, C., Montasser, M.E., Nag, A., Nakatuchi, M., Noce, D., Noordam, R., Pistis,  
1032 G., Preuss, M., Raffield, L., Rasmussen-Torvik, L.J., Rich, S.S., Robertson, N.R., Rueedi, R., Ryan,  
1033 K., Sanna, S., Saxena, R., Schraut, K.E., Sennblad, B., Setoh, K., Smith, A.V., Sparsø, T.,  
1034 Strawbridge, R.J., Takeuchi, F., Tan, J., Trompet, S., van den Akker, E., van der Most, P.J.,  
1035 Verweij, N., Vogel, M., Wang, H., Wang, C., Wang, N., Warren, H.R., Wen, W., Wilsgaard, T.,  
1036 Wong, A., Wood, A.R., Xie, T., Zafarmand, M.H., Zhao, J.-H., Zhao, W., Amin, N., Arzumanyan,  
1037 Z., Astrup, A., Bakker, S.J.L., Baldassarre, D., Beekman, M., Bergman, R.N., Bertoni, A., Blüher,  
1038 M., Bonnycastle, L.L., Bornstein, S.R., Bowden, D.W., Cai, Q., Campbell, A., Campbell, H.,  
1039 Chang, Y.C., de Geus, E.J.C., Dehghan, A., Du, S., Eiriksdottir, G., Farmaki, A.E., Fränberg, M.,  
1040 Fuchsberger, C., Gao, Y., Gjesing, A.P., Goel, A., Han, S., Hartman, C.A., Herder, C., Hicks, A.A.,  
1041 Hsieh, C.-H., Hsueh, W.A., Ichihara, S., Igase, M., Ikram, M.A., Johnson, W.C., Jørgensen, M.E.,  
1042 Joshi, P.K., Kalyani, R.R., Kandeel, F.R., Katsuya, T., Khor, C.C., Kiess, W., Kolcic, I.,  
1043 Kuulasmaa, T., Kuusisto, J., Läll, K., Lam, K., Lawlor, D.A., Lee, N.R., Lemaitre, R.N., Li, H.,  
1044 Lifelines Cohort Study, Lin, S.-Y., Lindström, J., Linneberg, A., Liu, J., Lorenzo, C., Matsubara,  
1045 T., Matsuda, F., Migrone, G., Mooijaart, S., Moon, S., Nabika, T., Nadkarni, G.N., Nadler, J.L.,  
1046 Nelis, M., Neville, M.J., Norris, J.M., Ohyagi, Y., Peters, A., Peyser, P.A., Polasek, O., Qi, Q.,  
1047 Raven, D., Reilly, D.F., Reiner, A., Rivideneira, F., Roll, K., Rudan, I., Sabanayagam, C., Sandow,  
1048 K., Sattar, N., Schürrmann, A., Shi, J., Stringham, H.M., Taylor, K.D., Teslovich, T.M., Thuesen,  
1049 B., Timmers, P.R.H.J., Tremoli, E., Tsai, M.Y., Uitterlinden, A., van Dam, R.M., van Heemst, D.,  
1050 van Hylckama Vlieg, A., van Vliet-Ostaptchouk, J.V., Vangipurapu, J., Vestergaard, H., Wang,  
1051 T., Willems van Dijk, K., Zemunik, T., Abecasis, G.R., Adair, L.S., Aguilar-Salinas, C.A.,  
1052 Alarcón-Riquelme, M.E., An, P., Aviles-Santa, L., Becker, D.M., Beilin, L.J., Bergmann, S.,  
1053 Bisgaard, H., Black, C., Boehnke, M., Boerwinkle, E., Böhm, B.O., Bønnelykke, K., Boomsma,  
1054 D.I., Bottinger, E.P., Buchanan, T.A., Canouil, M., Caulfield, M.J., Chambers, J.C., Chasman, D.I.,  
1055 Chen, Y.-D.I., Cheng, C.-Y., Collins, F.S., Correa, A., Cucca, F., de Silva, H.J., Dedoussis, G.,  
1056 Elmstähl, S., Evans, M.K., Ferrannini, E., Ferrucci, L., Florez, J.C., Franks, P.W., Frayling, T.M.,  
1057 Froguel, P., Gigante, B., Goodarzi, M.O., Gordon-Larsen, P., Grallert, H., Grarup, N., Grimsgaard,  
1058 S., Groop, L., Gudnason, V., Guo, X., Hamsten, A., Hansen, T., Hayward, C., Heckbert, S.R.,  
1059 Horta, B.L., Huang, W., Ingelsson, E., James, P.S., Jarvelin, M.-R., Jonas, J.B., Jukema, J.W.,  
1060 Kaleebu, P., Kaplan, R., Kardia, S.L.R., Kato, N., Keinanen-Kiukaanniemi, S.M., Kim, B.-J.,  
1061 Kivimaki, M., Koistinen, H.A., Kooner, J.S., Körner, A., Kovacs, P., Kuh, D., Kumari, M., Katalik,  
1062 Z., Laakso, M., Lakka, T.A., Launer, L.J., Leander, K., Li, H., Lin, X., Lind, L., Lindgren, C., Liu,  
1063 S., Loos, R.J.F., Magnusson, P.K.E., Mahajan, A., Metspalu, A., Mook-Kanamori, D.O., Mori,  
1064 T.A., Munroe, P.B., Njølstad, I., O'Connell, J.R., Oldehinkel, A.J., Ong, K.K., Padmanabhan, S.,  
1065 Palmer, C.N.A., Palmer, N.D., Pedersen, O., Pennell, C.E., Porteous, D.J., Pramstaller, P.P.,  
1066 Province, M.A., Psaty, B.M., Qi, L., Raffel, L.J., Rauramaa, R., Redline, S., Ridker, P.M.,  
1067 Rosendaal, F.R., Saaristo, T.E., Sandhu, M., Saramies, J., Schneiderman, N., Schwarz, P., Scott,  
1068 L.J., Selvin, E., Sever, P., Shu, X.-O., Slagboom, P.E., Small, K.S., Smith, B.H., Snieder, H., Sofer,  
1069 T., Sørensen, T.I.A., Spector, T.D., Stanton, A., Steves, C.J., Stumvoll, M., Sun, L., Tabara, Y.,  
1070 Tai, E.S., Timpson, N.J., Tönjes, A., Tuomilehto, J., Tusie, T., Uusitupa, M., van der Harst, P.,  
1071 van Duijn, C., Vitart, V., Vollenweider, P., Vrijkotte, T.G.M., Wagenknecht, L.E., Walker, M.,  
1072 Wang, Y.X., Wareham, N.J., Watanabe, R.M., Watkins, H., Wei, W.B., Wickremasinghe, A.R.,  
1073 Willemsen, G., Wilson, J.F., Wong, T.-Y., Wu, J.-Y., Xiang, A.H., Yanek, L.R., Yengo, L., Yokota,  
1074 M., Zeggini, E., Zheng, W., Zonderman, A.B., Rotter, J.I., Glyn, A.L., McCarthy, M.I., Dupuis,  
1075 J., Meigs, J.B., Scott, R.A., Prokopenko, I., Leong, A., Liu, C.-T., Parker, S.C.J., Mohlke, K.L.,  
1076 Langenberg, C., Wheeler, E., Morris, A.P., Barroso, I., and Meta-Analysis of Glucose and Insulin-  
1077 related Traits Consortium (MAGIC) (2021). The trans-ancestral genomic architecture of glycemic  
1078 traits. *Nat. Genet.* 53, 840–860.

1079 68. Molendijk, J., Blazev, R., Mills, R.J., Ng, Y.-K., Watt, K.I., Chau, D., Gregorevic, P., Crouch, P.J.,  
1080 Hilton, J.B.W., Lisowski, L., Zhang, P., Reue, K., Lusis, A.J., Hudson, J.E., James, D.E., Seldin,  
1081 M.M., and Parker, B.L. (2022). Proteome-wide systems genetics identifies UFMylation as a  
1082 regulator of skeletal muscle function. *Elife* 11. 10.7554/eLife.82951.

1083 69. Attwood, M.M., Fabbro, D., Sokolov, A.V., Knapp, S., and Schiöth, H.B. (2021). Trends in kinase  
1084 drug discovery: targets, indications and inhibitor design. *Nat. Rev. Drug Discov.* *20*, 839–861.

1085 70. Eduati, F., Jaaks, P., Wappler, J., Cramer, T., Merten, C.A., Garnett, M.J., and Saez-Rodriguez, J.  
1086 (2020). Patient-specific logic models of signalling pathways from screenings on cancer biopsies to  
1087 prioritize personalized combination therapies. *Mol. Syst. Biol.* *16*, e8664.

1088 71. Montagud, A., Béal, J., Tobalina, L., Traynard, P., Subramanian, V., Szalai, B., Alföldi, R., Puskás,  
1089 L., Valencia, A., Barillot, E., Saez-Rodriguez, J., and Calzone, L. (2022). Patient-specific Boolean  
1090 models of signalling networks guide personalised treatments. *Elife* *11*. 10.7554/eLife.72626.

1091 72. Houstis, N., Rosen, E.D., and Lander, E.S. (2006). Reactive oxygen species have a causal role in  
1092 multiple forms of insulin resistance. *Nature* *440*, 944–948.

1093 73. Fazakerley, D.J., Minard, A.Y., Krycer, J.R., Thomas, K.C., Stöckli, J., Harney, D.J., Burchfield,  
1094 J.G., Maghzal, G.J., Caldwell, S.T., Hartley, R.C., Stocker, R., Murphy, M.P., and James, D.E.  
1095 (2018). Mitochondrial oxidative stress causes insulin resistance without disrupting oxidative  
1096 phosphorylation. *J. Biol. Chem.* *293*, 7315–7328.

1097 74. Su, Z., Burchfield, J.G., Yang, P., Humphrey, S.J., Yang, G., Francis, D., Yasmin, S., Shin, S.-Y.,  
1098 Norris, D.M., Kearney, A.L., Astore, M.A., Scavuzzo, J., Fisher-Wellman, K.H., Wang, Q.-P.,  
1099 Parker, B.L., Neely, G.G., Vafaee, F., Chiu, J., Yeo, R., Hogg, P.J., Fazakerley, D.J., Nguyen, L.K.,  
1100 Kuyucak, S., and James, D.E. (2019). Global redox proteome and phosphoproteome analysis  
1101 reveals redox switch in Akt. *Nat. Commun.* *10*, 5486.

1102 75. Piazza, I., Kochanowski, K., Cappelletti, V., Fuhrer, T., Noor, E., Sauer, U., and Picotti, P. (2018).  
1103 A Map of Protein-Metabolite Interactions Reveals Principles of Chemical Communication. *Cell*  
1104 *172*, 358–372.e23.

1105 76. Hicks, K.G., Cluntun, A.A., Schubert, H.L., Hackett, S.R., Berg, J.A., Leonard, P.G., Ajalla Aleixo,  
1106 M.A., Zhou, Y., Bott, A.J., Salvatore, S.R., Chang, F., Blevins, A., Barta, P., Tilley, S., Leifer, A.,  
1107 Guzman, A., Arok, A., Fogarty, S., Winter, J.M., Ahn, H.-C., Allen, K.N., Block, S., Cardoso, I.A.,  
1108 Ding, J., Dreveny, I., Gasper, W.C., Ho, Q., Matsuura, A., Palladino, M.J., Prajapati, S., Sun, P.,  
1109 Tittmann, K., Tolan, D.R., Unterlass, J., VanDemark, A.P., Vander Heiden, M.G., Webb, B.A.,  
1110 Yun, C.-H., Zhao, P., Wang, B., Schopfer, F.J., Hill, C.P., Nonato, M.C., Muller, F.L., Cox, J.E.,  
1111 and Rutter, J. (2023). Protein-metabolite interactomics of carbohydrate metabolism reveal  
1112 regulation of lactate dehydrogenase. *Science* *379*, 996–1003.

1113 77. Sano, H., Kane, S., Sano, E., Miinea, C.P., Asara, J.M., Lane, W.S., Garner, C.W., and Lienhard,  
1114 G.E. (2003). Insulin-stimulated phosphorylation of a Rab GTPase-activating protein regulates  
1115 GLUT4 translocation. *J. Biol. Chem.* *278*, 14599–14602.

1116 78. Parks, B.W., Sallam, T., Mehrabian, M., Psychogios, N., Hui, S.T., Norheim, F., Castellani, L.W.,  
1117 Rau, C.D., Pan, C., Phun, J., Zhou, Z., Yang, W.-P., Neuhaus, I., Gargalovic, P.S., Kirchgessner,  
1118 T.G., Graham, M., Lee, R., Tontonoz, P., Gerszten, R.E., Hevener, A.L., and Lusis, A.J. (2015).  
1119 Genetic architecture of insulin resistance in the mouse. *Cell Metab.* *21*, 334–347.

1120 79. Yardeni, T., Eckhaus, M., Morris, H.D., Huizing, M., and Hoogstraten-Miller, S. (2011). Retro-  
1121 orbital injections in mice. *Lab Anim.* *40*, 155–160.

1122 80. Goodner, C.J., Hom, F.G., and Berrie, M.A. (1980). Investigation of the effect of insulin upon  
1123 regional brain glucose metabolism in the rat *in vivo*. *Endocrinology* *107*, 1827–1832.

1124 81. Storey, J.D. (2002). A direct approach to false discovery rates. *J. R. Stat. Soc. Series B Stat.*  
1125 *Methodol.* *64*, 479–498.

1126 82. Carlson, M. (2019). org. Mm. eg. db: Genome wide annotation for Mouse. R package version 3.2.  
1127 3. Bioconductor. London, United Kingdom: Genome Biology (BMC).

1128 83. Carey, A.L., Steinberg, G.R., Macaulay, S.L., Thomas, W.G., Holmes, A.G., Ramm, G., Prelovsek,  
1129 O., Hohnen-Behrens, C., Watt, M.J., James, D.E., Kemp, B.E., Pedersen, B.K., and Febbraio, M.A.  
1130 (2006). Interleukin-6 increases insulin-stimulated glucose disposal in humans and glucose uptake  
1131 and fatty acid oxidation in vitro via AMP-activated protein kinase. *Diabetes* 55, 2688–2697.

1132 84. Krycer, J.R., Elkington, S.D., Diaz-Vegas, A., Cooke, K.C., Burchfield, J.G., Fisher-Wellman,  
1133 K.H., Cooney, G.J., Fazakerley, D.J., and James, D.E. (2020). Mitochondrial oxidants, but not  
1134 respiration, are sensitive to glucose in adipocytes. *J. Biol. Chem.* 295, 99–110.

1135 85. Masson, S.W.C., Woodhead, J.S.T., D’Souza, R.F., Broome, S.C., MacRae, C., Cho, H.C., Atiola,  
1136 R.D., Futi, T., Dent, J.R., Shepherd, P.R., and Merry, T.L. (2021).  $\beta$ -Catenin is required for optimal  
1137 exercise- and contraction-stimulated skeletal muscle glucose uptake. *J. Physiol.* 599, 3897–3912.

1138

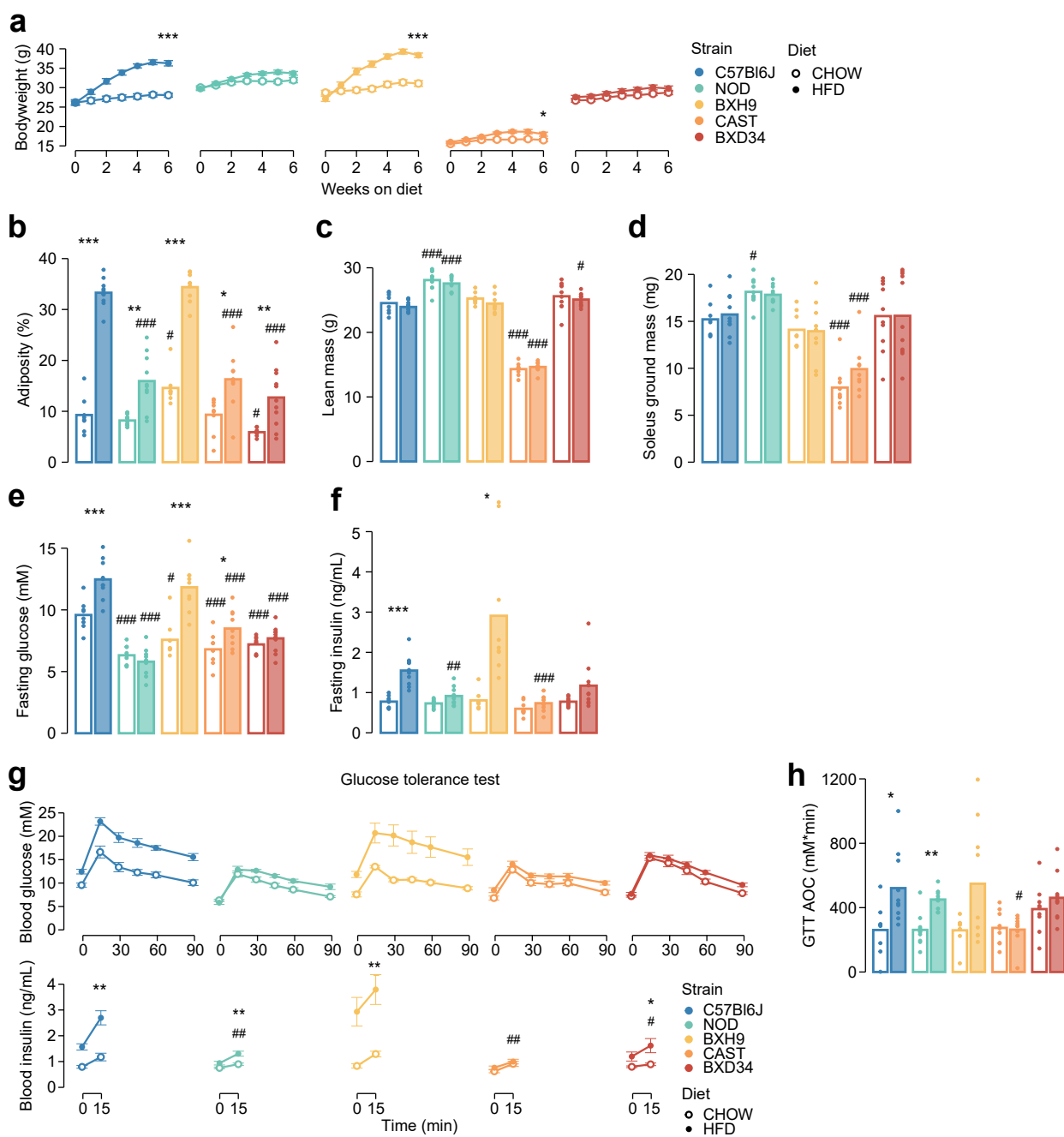


**Figure S1: Genetics and diet alter morphometric and metabolic phenotypes.** Related to Fig. 1.

**a)** Mouse bodyweight was measured during a six-week diet regimen. Two-sided t-tests were performed to compare HFD to CHOW within each strain after six weeks, following Benjamini-Hochberg p-value adjustment (\*). **b-d)** Measurement of **b)** adiposity, **c)** lean mass, **d)** ground soleus mass, **e)** fasting blood glucose, and **f)** fasting blood insulin at the end of the diet regimen. **g)** At the end of the diet regimen a glucose tolerance test was performed. **h)** The area of the blood glucose curve (GTT AOC) was calculated. In **b-h)**, two-sided t-tests were performed to compare HFD to CHOW within each strain (\*) or to compare each strain to C57Bl6J within either diet (#). P-values were adjusted by the Benjamini-Hochberg procedure. Error bars indicate SEM. In **g)** t-tests were only performed on 15-minute blood insulin levels. No comparisons across strains on CHOW were significant. n = 8-11 biological replicates. \*#/ #: 0.01 ≤ p < 0.05, \*\*/##: 0.001 ≤ p < 0.01, \*\*\*/###: p < 0.001

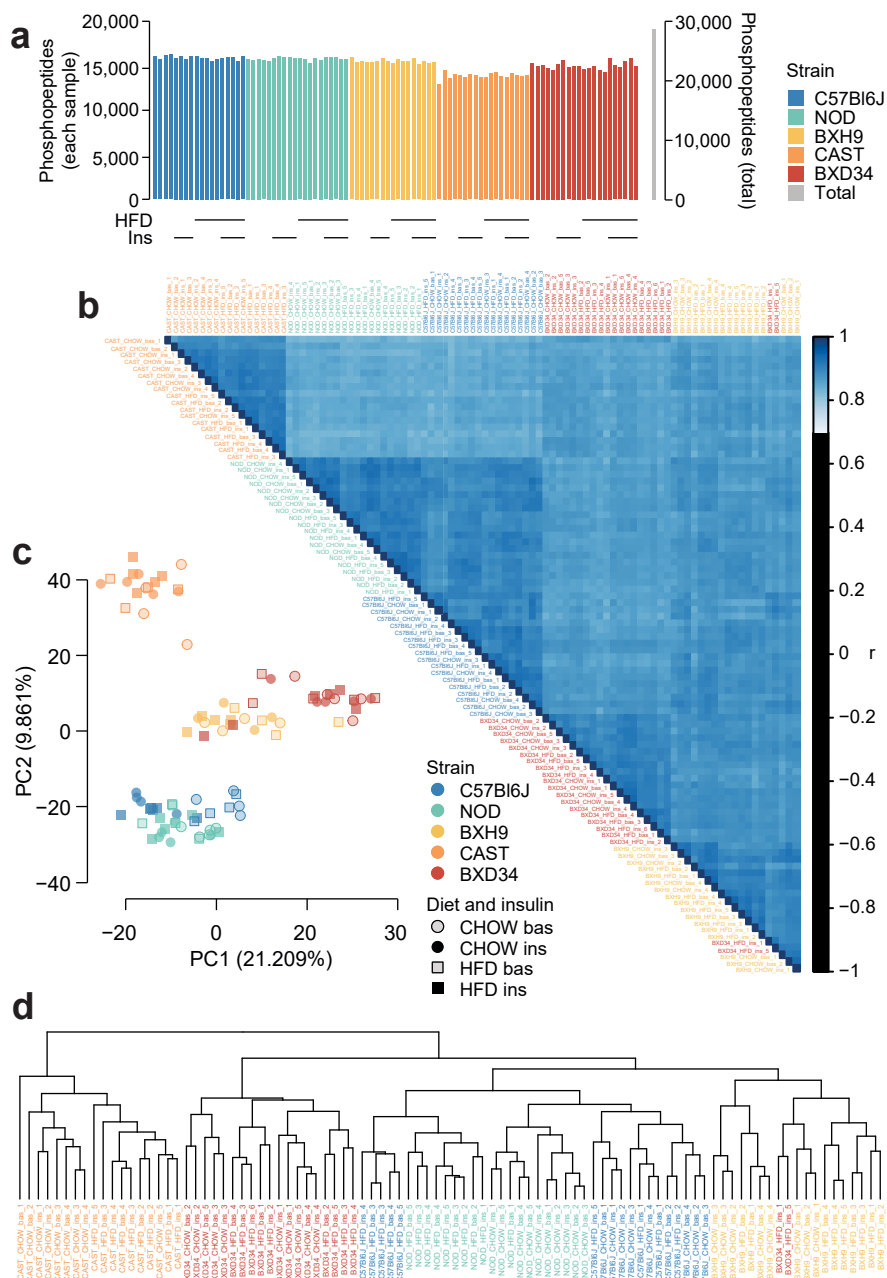


**Figure S2: Quality control analysis of phosphoproteomics data.** Related to Fig. 1. **a)** The number of unique class I phosphopeptides quantified in each sample and in total. **b)** Pearson's correlation was performed between each pair of samples. Samples are ordered by hierarchical clustering. **c)** Principal component analysis was performed on the phosphoproteome. The first two principal components (PC1 and PC2) are plotted for each sample and the percentage of overall variance explained by each principal component is indicated. “bas”: unstimulated, “ins”: insulin-stimulated. **d)** Hierarchical clustering was performed on all samples.

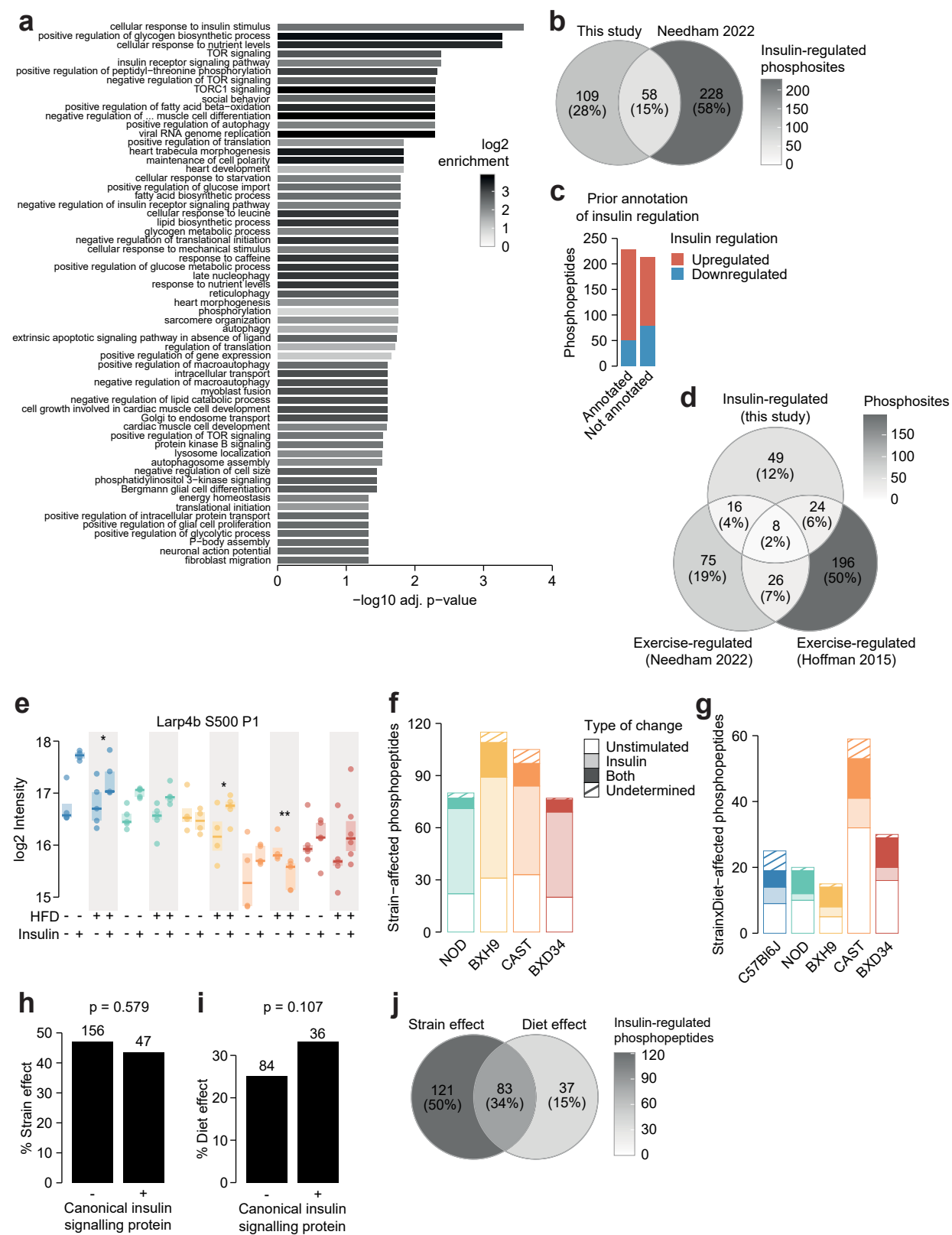


**Figure S3: Characterisation of the insulin-regulated phosphoproteome.** Related to Fig. 1-3. a)

The enrichment of GO biological processes in genes containing insulin-regulated phosphopeptides relative to the entire phosphoproteome (one-sided Fisher's exact test, Benjamini-Hochberg p-value adjustment). Only significant pathways are shown (adj.  $p < 0.05$ ). The pathway "negative regulation of vascular associated smooth muscle cell differentiation" is abbreviated. **b)** The number of phosphosites regulated by insulin in this study or a previous phosphoproteomic study of human skeletal muscle<sup>1</sup>. Only phosphosites quantified in both

studies were considered. **c)** The number of insulin-regulated phosphopeptides with prior annotation of insulin regulation in the PhosphositePlus database<sup>2</sup>. **d)** The number of phosphosites regulated by insulin this study or regulated by exercise in two human phosphoproteomics studies<sup>1,3</sup>. Only phosphosites quantified in all three studies were considered. **e)** A phosphopeptide where HFD-feeding enhanced insulin responses in BXH9 but suppressed insulin responses in C57Bl6J and CAST. A two-way ANOVA was performed on insulin response values followed by two-sided t-tests comparing HFD to CHOW within each strain (q-values: \*). **f)** Phosphopeptides with a Strain effect were examined to determine whether the effect was due to altered unstimulated phosphorylation (“Unstimulated”; Strain/C57Bl6J fold change > 1.3 in unstimulated samples), altered insulin-stimulated phosphorylation (“Insulin”; Strain/C57Bl6J fold change > 1.3 in insulin-stimulated samples), or both (“Both”). A proportion of phosphopeptides passed neither of these filters (“Undetermined”). **g)** The same analysis was performed on StrainxDiet-affected phosphopeptides, using the HFD/CHOW fold changes in either unstimulated or insulin-stimulated samples for each strain. **h-i)** The percentage of **h)** Strain effects and **i)** Diet effects (Uniform diet or StrainxDiet effect) among canonical or noncanonical insulin signalling proteins. P-values indicate two-sided Fisher’s exact tests. The number of phosphopeptides in each group is shown. **j)** The overlap of Strain and Diet effects.

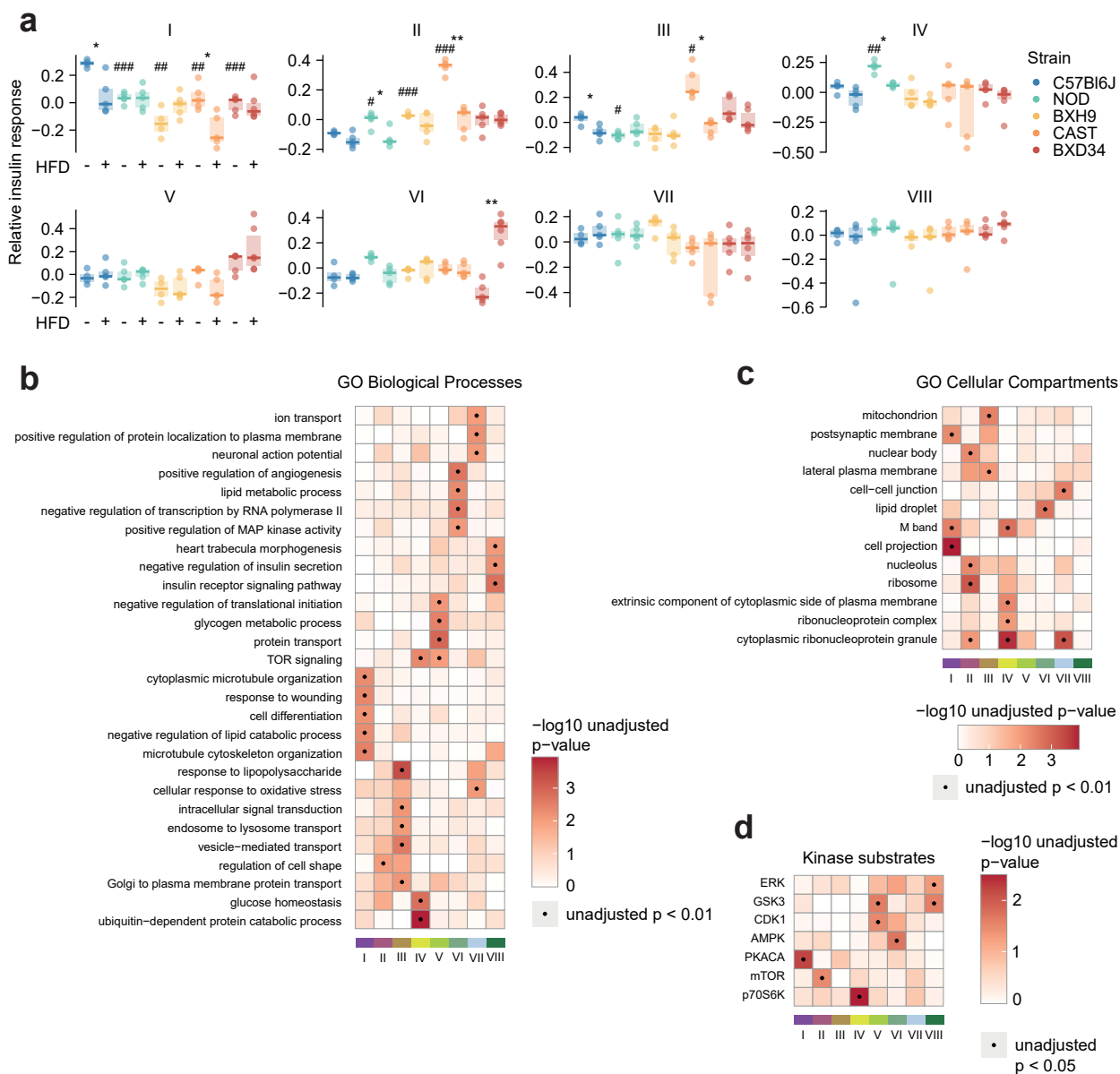


**Figure S4: Characterising insulin signalling subnetworks.** Related to Fig. 5. **a)** The eigenpeptides of each WGCNA-derived subnetwork. ANOVAs were performed on CHOW values following two-sided t-tests comparing each strain to C57Bl6J (Benjamini-Hochberg-adjusted p-values: #), and two-way ANOVAs were performed on all values followed by two-sided t-tests comparing HFD to CHOW within each strain (adjusted p-values: \*). **b-d)** Rank-based enrichment of GO biological pathways, GO cellular compartments, and PhosphositePlus kinase substrates using phosphopeptide module membership scores with the “geneSetTest” function from the R package “limma”. Membership score is defined as the absolute Pearson’s correlation coefficient between a phosphopeptide’s insulin response and the subnetwork’s eigenpeptide.

\*/#:  $0.01 \leq p < 0.05$ , \*\*/##:  $0.001 \leq p < 0.01$ , \*\*\*/###:  $p < 0.001$

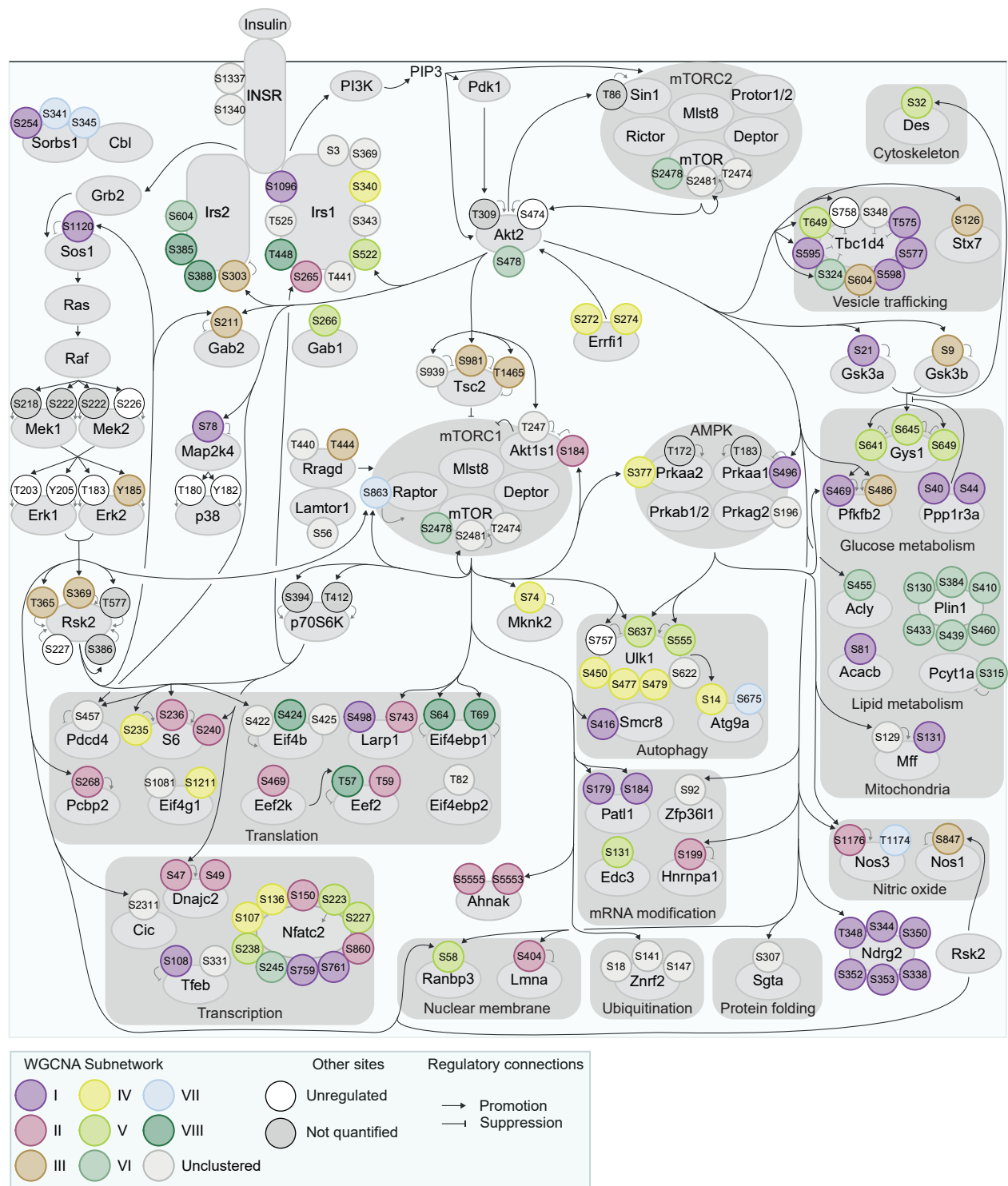


**Figure S5: Organisation of insulin signalling subnetworks.** Related to Fig. 5. The curated insulin signalling network displayed in Fig. 3 was annotated with WGCNA subnetworks from Fig. 5.

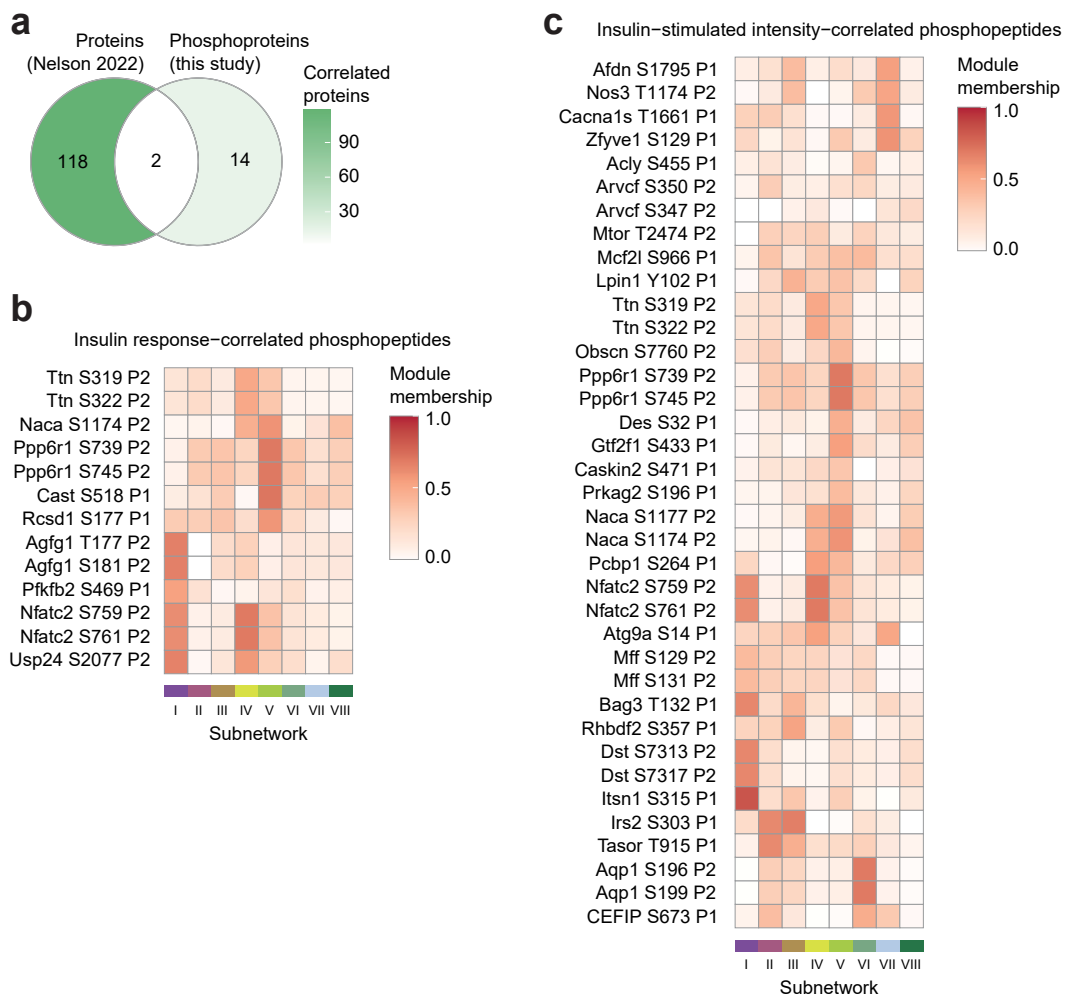


**Figure S6: Characterisation of glucose-uptake correlated phosphosites.** Related to Fig. 6. **a)** The intersection of proteins correlated with insulin-stimulated glucose uptake in the soleus of seven inbred mouse strains fed CHOW or HFD<sup>4</sup> ( $p < 0.1$ ,  $r > 0.35$  or  $< -0.35$ ), with proteins containing glucose-uptake correlated phosphopeptides in this study. Only (phospho)proteins quantified in both studies are shown. **b-c)** The subnetwork membership scores for glucose-uptake correlated phosphopeptides using **b)** insulin-stimulated phosphopeptide intensity, or **c)** phosphopeptide insulin response values. Membership score is defined as the absolute Pearson's correlation coefficient between a phosphopeptide's insulin response and the subnetwork's eigenpeptide.

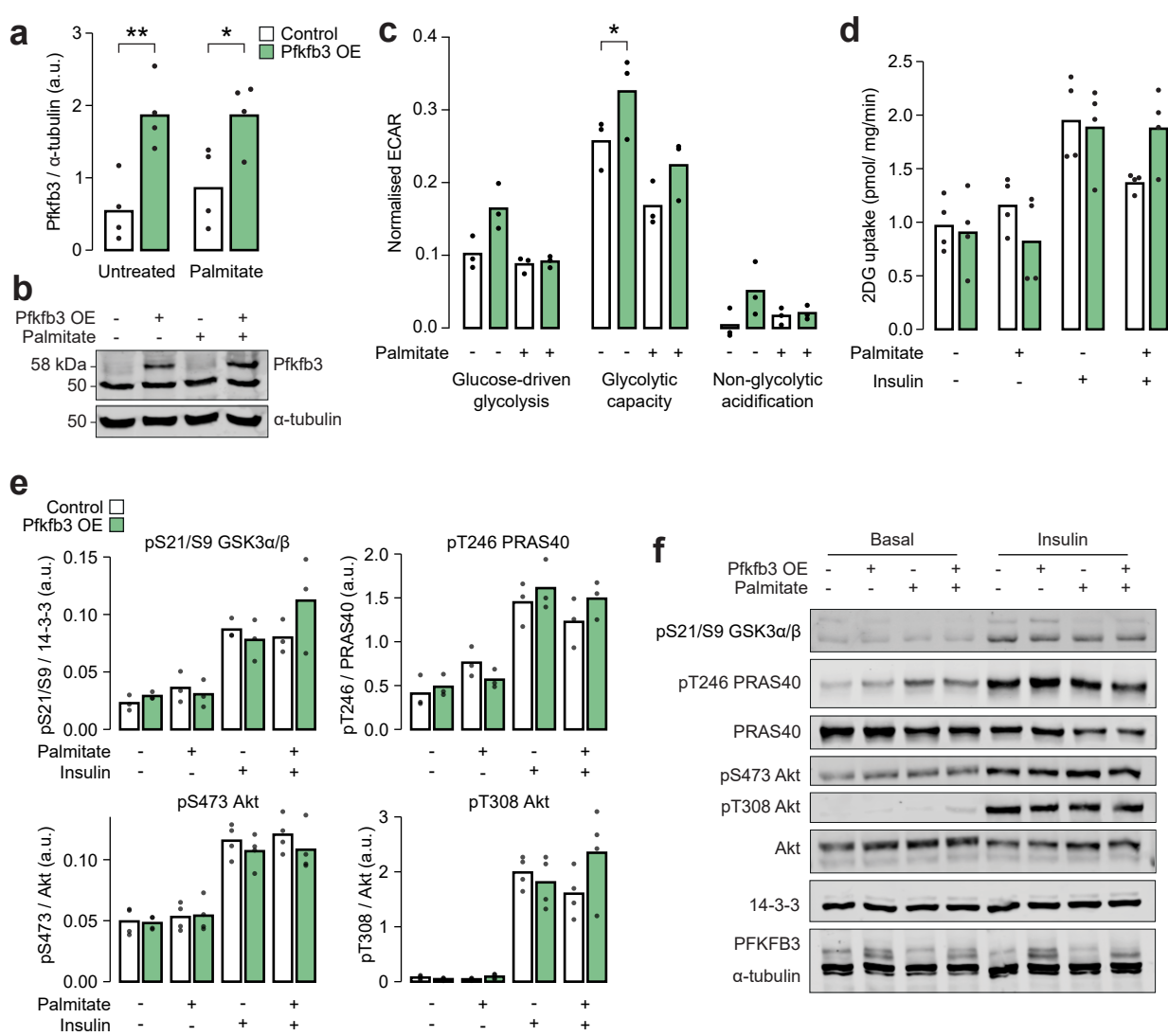


**Figure S7: Overexpression of Pfkfb3 enhances glycolytic capacity and reverses palmitate-induced insulin resistance.** Related to Fig. 6. **a)** Quantification and **b)** representative blot for immunoblotting of Pfkfb3 in L6-GLUT4-HA myotubes with or without Pfkfb3 overexpression, treated with palmitate (125  $\mu$ M, 16 h) or BSA vehicle control. Two-way ANOVA was performed followed by Šidák's post-hoc tests assessing the effect of Pfkfb3 overexpression (\*). n = 4 biological replicates. **c)** Extracellular acidification rate (ECAR) in L6-GLUT4-HA myotubes treated with glucose (10 mM, “Glucose-driven glycolysis”), oligomycin (5  $\mu$ g/mL, “Glycolytic capacity”), or 2-deoxyglucose (50 mM, “Non-glycolytic acidification”). A two-way ANOVA was performed followed by Tukey's posthoc tests comparing conditions within each of the three treatments (\*). Not all significant comparisons are shown. n = 3 biological replicates. **d)** Unstimulated and insulin-stimulated glucose uptake (100 nM insulin, 20 min) in L6-GLUT4-HA myotubes. Insulin/unstimulated fold changes are shown in **Fig. 6h**. **e)** Quantification and **f)** representative blot for immunoblotting of insulin signalling phosphosites in unstimulated or insulin-stimulated (100 nM, 20 min) L6-GLUT4-HA myotubes.

\*/#: 0.01  $\leq$  p  $<$  0.05, \*\*/##: 0.001  $\leq$  p  $<$  0.01, \*\*\*/###: p  $<$  0.001

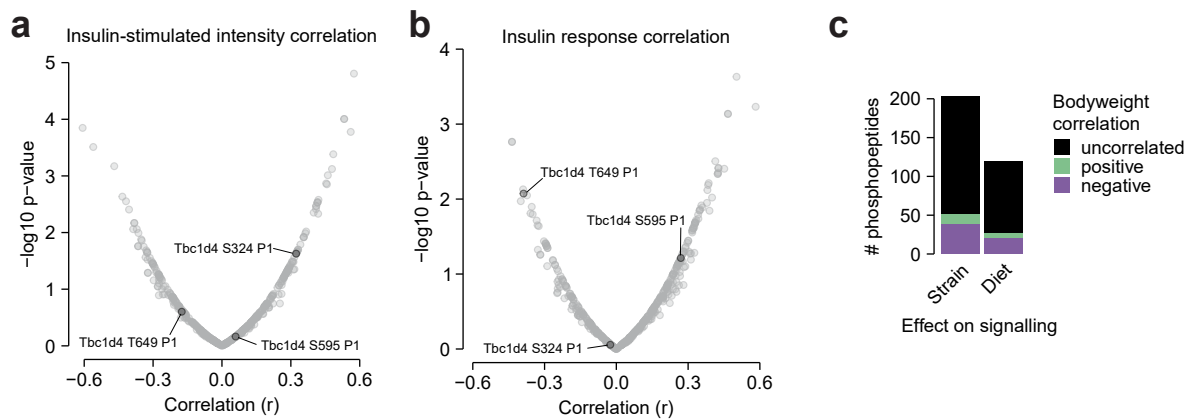


**Figure S8: Additional glucose uptake correlation analysis.** Related to Discussion. **a-b)** The correlation of insulin-stimulated glucose uptake with insulin-regulated phosphopeptides using **a)** insulin-stimulated phosphopeptide intensity, or **b)** phosphopeptide insulin response values, as displayed in **Fig. 6**. Canonical regulatory phosphosites on Tbc1d4 are indicated. The fourth canonical regulatory site S758 was not analysed due to insufficient quantification (quantified in 4/94 samples). **c)** The correlation of mouse bodyweight with the insulin responses of Strain or Diet-affected phosphopeptides either in CHOW-fed mice (Strain effects) or across both diets (Diet effects). The number of positively correlated (Pearson's correlation,  $q < 0.1$ ,  $r > 0.35$ ) and negatively correlated ( $q < 0.1$ ,  $r < -0.35$ ) phosphopeptides is shown.

***Table S1: Muscle phosphoproteomics***

(Page 1 “01\_quantification”) Normalized LFQ intensities of class I phosphopeptides. (Page 2 “02\_analysis”) Statistical analysis of phosphoproteome data.

***Table S2: Overlap between insulin and exercise-regulated phosphosites***

Insulin-regulated phosphosites from this study that were additionally regulated by exercise either in Needham et al.<sup>1</sup> or Hoffman et al.<sup>3</sup>.

<b>Phosphosite details</b>				<b>Exercise regulation</b>			
<b>PhosphositePlus</b>		<b>Site Group ID</b>	<b>Gene</b>	<b>Uniprot</b>	<b>Phosphosite</b>	<b>Hoffman 2015</b>	<b>Needham 2022</b>
		450254	Eef2	P58252	T59	+	+
		448040	Eef2	P58252	T57	+	+
		470754	Mff	Q6PCP5	S131	+	+
		470753	Mff	Q6PCP5	S129	+	+
		453632	Larp1	Q6ZQ58	S498	+	+
		455925	Tbc1d4	Q8BYJ6	S324	+	+
		4762876	Svil	Q8K4L3	S300	+	+
		448238	Gys1	Q9Z1E4	S645	+	+
		480145	Tns1	E9Q0S6	S1054	+	
		3176152	Ulk1	O70405	S450	+	
		448064	Rps6ka3	P18654	S369	+	
		469782	Dnajc2	P54103	S47	+	
		486522	Pcbp1	P60335	S264	+	
		448094	Rps6	P62754	S240	+	
		448093	Rps6	P62754	S236	+	
		447594	Mapk1	P63085	Y185	+	
		453577	Patl1	Q3TC46	S179	+	
		447527	Eif4ebp1	Q60876	S64	+	
		482918	Pcbp2	Q61990	S268	+	
		4731870	Speg	Q62407	S542	+	
		14570198	Atg9a	Q68FE2	S675	+	
		455922	Tbc1d4	Q8BYJ6	S348	+	
		471364	Lpin1	Q91ZP3	S923	+	
		448239	Gys1	Q9Z1E4	S649	+	
		4693547	Ttn	A2ASS6	S322		+
		480195	Usp24	B1AY13	S1296		+
		10782556	Usp24	B1AY13	S1282		+
		483808	Akap13	E9Q394	S2692		+
		3208338	Akap1	O08715	S103		+
		3831732	Tom1	O88746	S376		+
		2048085	Rab12	P35283	S20		+
		447655	Map2k4	P47809	S78		+
		4720237	Lmod2	Q3UHZ5	T391		+
		450706	Hspb6	Q5EBG6	S16		+
		4726016	Tom1l2	Q5SRX1	S394		+
		4716961	Slc20a2	Q80UP8	S316		+
		17544627	Lmod1	Q8BVA4	S511		+
		11180047	Tbc1d4	Q8BYJ6	S604		+
		455921	Tbc1d4	Q8BYJ6	T649		+
		3195560	Golga4	Q91VW5	S41		+
		485723	Plekhf2	Q91WB4	S226		+
		4772204	Ehbp1l1	Q99MS7	S1460		+
		470067	Akt1s1	Q9D1F4	T247		+
		452430	Plec	Q9QXS1	S4620		+

451009 Ndrg2	Q9QYG0	T348	+
468257 Ndrg2	Q9QYG0	S338	+
468259 Ndrg2	Q9QYG0	S344	+
447886 Nos1	Q9Z0J4	S847	+

**Table S3: Insulin signalling subnetworks**

WGCNA-derived subnetworks of insulin-regulated phosphopeptides.

**Table S4: Association of kinase enrichment with insulin-stimulated glucose uptake**

Pearson's correlation of KSEA enrichment scores with insulin-stimulated glucose uptake for all kinases with Strain or Diet effects. Correlation was performed on all values or on the medians of each Strain-Diet combination.

Kinase	Correlating all values		Correlating Strain-Diet medians	
	r	p	r	p
SGK	0.026282557	0.85773407	-0.114513813	0.752760165
Aur	0.181856398	0.221176679	0.446186208	0.196168185
p90RSK	0.042637179	0.771137201	0.392619919	0.261741297
aPKC	0.020857899	0.886881337	0.059269839	0.870801728
GSK3	-0.023496391	0.872683503	0.200939915	0.577765996
CDK5	0.092355979	0.527940053	0.136553891	0.706796386
P38	0.186315084	0.199914602	0.202333014	0.575075383
CDK1	0.134654975	0.356287427	0.245970422	0.493328434
CK2	0.062152944	0.671383691	-0.206449396	0.567152858

## Supplementary references

1. Needham, E.J., Hingst, J.R., Parker, B.L., Morrison, K.R., Yang, G., Onslev, J., Kristensen, J.M., Højlund, K., Ling, N.X.Y., Oakhill, J.S., Richter, E.A., Kiens, B., Petersen, J., Pehmøller, C., James, D.E., Wojtaszewski, J.F.P., and Humphrey, S.J. (2021). Personalized phosphoproteomics identifies functional signaling. *Nat. Biotechnol.* 10.1038/s41587-021-01099-9.
2. Hornbeck, P.V., Zhang, B., Murray, B., Kornhauser, J.M., Latham, V., and Skrzypek, E. (2015). PhosphoSitePlus, 2014: mutations, PTMs and recalibrations. *Nucleic Acids Res.* 43, D512-20.
3. Hoffman, N.J., Parker, B.L., Chaudhuri, R., Fisher-Wellman, K.H., Kleinert, M., Humphrey, S.J., Yang, P., Holliday, M., Trefely, S., Fazakerley, D.J., Stöckli, J., Burchfield, J.G., Jensen, T.E., Jothi, R., Kiens, B., Wojtaszewski, J.F.P., Richter, E.A., and James, D.E. (2015). Global Phosphoproteomic Analysis of Human Skeletal Muscle Reveals a Network of Exercise-Regulated Kinases and AMPK Substrates. *Cell Metab.* 22, 922–935.
4. Nelson, M.E., Madsen, S., Cooke, K.C., Fritzen, A.M., Thorius, I.H., Masson, S.W.C., Carroll, L., Weiss, F.C., Seldin, M.M., Potter, M., Hocking, S.L., Fazakerley, D.J., Brandon, A.E., Thillainadesan, S., Senior, A.M., Cooney, G.J., Stöckli, J., and James, D.E. (2022). Systems-level analysis of insulin action in mouse strains provides insight into tissue- and pathway-specific interactions that drive insulin resistance. *Cell Metab.* 34, 227-239.e6.